Chapter 17
Planar Four-Bar Mechanism

The solid lines in Fig. 17.1 are the links of a planar four-bar mechanism or briefly planar four-bar. The link lengths ℓ (base or fixed link), r_1 (input link), r_2 (output link) and a (coupler) are free parameters. They determine, whether individual links can rotate relative to others full cycle (i.e., unlimited) or through an angle smaller than 2π. The link lengths also determine the so-called transfer function relating the output angle ψ to the input angle φ. The time derivative of this function yields the *transmission ratio* $i = \dot{\varphi}/\dot{\psi}$ as function of φ. The transfer function and the transmission ratio depend on three parameters only, namely, on r_1/ℓ, r_2/ℓ and a/ℓ. Points fixed in the plane of the coupler move along *coupler curves*. The shapes of these curves depend on six parameters, namely, on the four link lengths and, in addition, on two coordinates of the coupler-fixed point in the coupler plane. The coupler plane as a whole undergoes a translatory-rotatory motion through a continuum of positions which depends on the four link lengths. The said dependencies which are the subject of the following sections are highly complicated. It is this complexity in combination with simplicity of design which makes the planar four-bar the most important linkage in engineering.

Literature on four-bars and on other linkages: Erdman (Ed.) [11], Artobolevski [1], Geronimus [16], Dijksman [10].

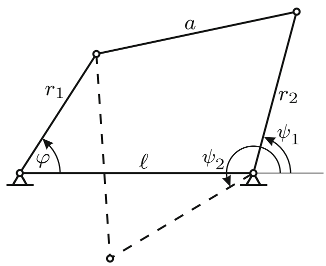

Fig. 17.1 Planar four-bar in the two positions existing for a given input angle φ

© Springer-Verlag Berlin Heidelberg 2016

J. Wittenburg, *Kinematics*, DOI 10.1007/978-3-662-48487-6_17

In many machines a certain desired property is achieved by combining a four-bar with additional elements. A typical example is shown in Fig. 17.2. Without the motor-driven crank mechanism MDB drawn with dashed lines the mechanism is a four-bar A_0ABB_0 with base A_0B_0. None of its links is able to rotate full cycle relative to the base. When this four-bar is moving through its entire range, the coupler-fixed point C traces the dotted coupler curve. A section of this curve is a very good straight-line approximation. The combination of the four-bar A_0ABB_0 with the crank mechanism MDB results in a machine in which C is moving periodically back and forth the straight section when the crank is rotating. Point C can be used as guide for the piston of the pump at an oil-well.

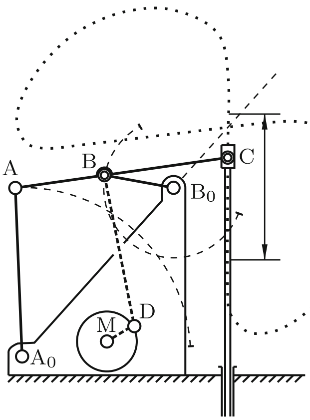

Fig. 17.2 Combination of four-bar and crank mechanism in a pump

17.1 Grashof Condition

In this section answers are given to the following questions. Through which angle can two neighboring links of a four-bar rotate relative to each other? Under which condition is this angle unlimited? In this case, one link is said to be fully rotating relative to the other. For every possible angle φ between two neighboring links there exist two positions of the four-bar (see Fig. 17.1). In some four-bars the transition from one of these positions into the other can be achieved by a continuous motion. In others the transition is possible only by disconnecting and reassembling the four-bar. Under which conditions is disconnection and reassembly necessary? The properties addressed by these questions do not depend on which link is chosen as fixed link and which as input link. Arbitrarily, the angle φ of the link of length r_1 against the

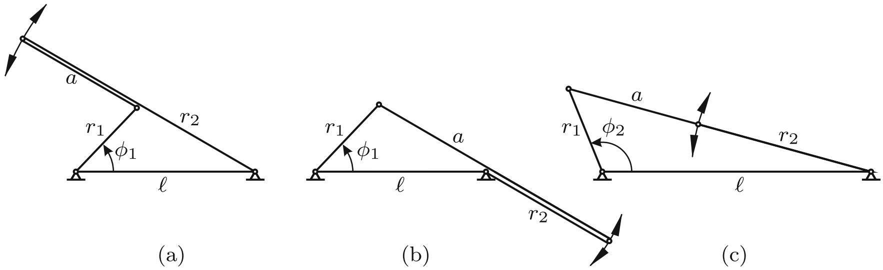

Fig. 17.3 Limit positions of a four-bar

link of length ℓ is investigated. Extremal values of φ in limit positions are denoted ϕ. In Figs. 17.3a,b,c all possible configurations in limit positions are shown. All of them are characterized by collinearity of the other two links of the four-bar. For the extremal angles ϕ_1 and ϕ_2 the cosine law yields the expressions

$$\cos\phi_{1,2} = \frac{r_1^2 + \ell^2 - (r_2 \mp a)^2}{2r_1\ell} \, . \tag{17.1}$$

The links are fully rotating relative to each other if $\cos\phi_1 \geq +1$ as well as $\cos\phi_2 \leq -1$. These conditions are

$$\text{a)} \quad |r_1 - \ell| \geq |r_2 - a| \, , \qquad \text{b)} \quad r_1 + \ell \leq r_2 + a \, . \tag{17.2}$$

In the special case of four identical link lengths $\ell = r_1 = r_2 = a \quad \phi_1 = 0$, $\phi_2 = \pi$. This means that neighboring links can rotate full cycle relative to each other.

In what follows, it is assumed that at least two link lengths are different. Let $\ell_{\min}$ and $\ell_{\max} \neq \ell_{\min}$ be the smallest and the largest, respectively, of the four link lengths, and let ℓ' and ℓ'' ($\ell' < \ell''$ or $\ell' = \ell''$ or $\ell' > \ell''$) be the other two link lengths so that

$$\ell_{\min} \leq \ell', \; \ell'' \leq \ell_{\max} \qquad (\ell_{\max} \neq \ell_{\min}) \, . \tag{17.3}$$

Grashof[1] [17] is the author of

Theorem 17.1. *The link of length $\ell_{\min}$ is fully rotating relative to all other links if and only if the condition*

$$\ell_{\min} + \ell_{\max} \leq \ell' + \ell'' \tag{17.4}$$

[1] F. Grashof 1826-1893, professor at the *Polytechnische Schule Karlsruhe*, now Karlsruhe Institute of Technology (KIT); one of the founders and first chairman of *Verein Deutscher Ingenieure* (VDI)

is satisfied. Then these other links are fully rotating relative to the link with $\ell_{\min}$ *, but they are not fully rotating relative to each other. If condition (17.4) is not satisfied, no link is fully rotating relative to any other link.*

Proof: The following statements are easily verified if not obvious.
I. Equations (17.1) as well as conditions (17.2a,b) are invariant with respect to an interchange of r_1 and ℓ and also of r_2 and a.
II. If neither r_1 nor ℓ is $\ell_{\min}$, one of the conditions (17.2a), (17.2b) is violated.
III. If either (r_1, ℓ) or (ℓ, r_1) is the pair $(\ell_{\min}, \ell_{\max})$, condition (17.2a) is satisfied, and condition (17.2b) is condition (17.4).
IV. If either (r_1, ℓ) or (ℓ, r_1) is the pair $(\ell_{\min}, \ell')$, condition (17.2b) is satisfied, and condition (17.2a) is condition (17.4).
The combination of statements I to IV proves Grashof's theorem. According to this theorem four-bars are divided into

- four-bars satisfying Grashof's condition; these four-bars are further subdivided
  - general case: $\ell_{\min} + \ell_{\max} < \ell' + \ell''$
  - special case: $\ell_{\min} + \ell_{\max} = \ell' + \ell''$
- four-bars not satisfying Grashof's condition, i.e., four-bars with $\ell_{\min} + \ell_{\max} > \ell' + \ell''$.

Matters are even more complicated due to the fact that in engineering practice a particular link of a four-bar is declared to be the fixed link. A neighboring link (input link or output link) is referred to as *crank* or as *rocker* depending on whether or not it is fully rotating relative to the fixed link. Depending on the behavior of input link and output link a four-bar is either a *double-crank* or a *crank-rocker* or a *double-rocker*. It is obvious that a four-bar not satisfying Grashof's condition is a double-rocker. On the other hand, a four-bar satisfying Grashof's condition may be either a *double-crank* or a *crank-rocker* or a *double-rocker*. Details are worked out in what follows.

Four-Bars Satisfying Grashof's Inequality Condition $\ell_{\min} + \ell_{\max} < \ell' + \ell''$. For demonstration the link lengths (3, 5, 6, 7) are used which satisfy Grashof's condition $(3 + 7 < 5 + 6)$. In Fig. 17.4a the fixed link is the shortest link. This link (and only this link) is fully rotating relative to all other links. In other words: The input link, the output link and the coupler are fully rotating relative to the fixed link. Hence the four-bar is a *double-crank*. For a single input angle the two existing positions of the four-bar are shown (one of them with dashed lines).

In Fig. 17.4b the input link is the shortest link. Only this link is fully rotating relative to all other links. Hence the four-bar is a *crank-rocker*. The four-bar is shown in all four limit positions of the rocker. The angular range of the rocker consists of two sectors $< 180°$ which are arranged symmetrically to the base line. The base line is outside these sectors. For a single input angle the two existing positions of the four-bar are shown (one of them with

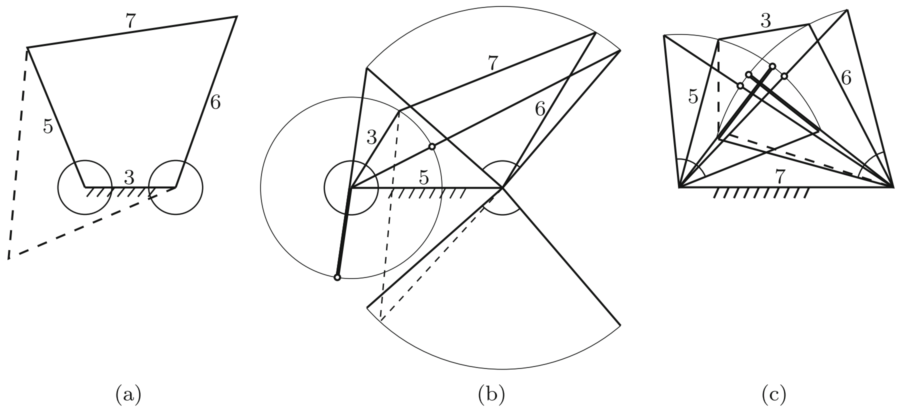

Fig. 17.4 Four-bars with different distributions of the link lengths (3, 5, 6, 7). Double-crank (**a**) with all links fully rotating. Crank-rocker (**b**) with fully rotating input crank. Double-rocker of first kind with fully rotating coupler (**c**)

dashed lines). In these two positions the output link is located on opposite sides of the base line.

Figure 17.4c differs from Fig. 17.4a in that the fixed link and the coupler are interchanged. The coupler is the shortest link. Only the coupler is fully rotating relative to all other links. The four-bar is referred to as *double-rocker of first kind*. The figure shows the limit positions of both rockers. The angular range of each rocker is a single sector. The sectors of both rockers are on one and the same side of the base line. For a single input angle the two existing positions of the four-bar are shown (one of them with dashed lines). In these two positions the output link is located on one and the same side of the base line.

In Figs. 17.4a , b and c reflection of every possible position in the base line is another possible position.

Four-Bars not Satisfying Grashof's Condition
For demonstration the link lengths (4, 5, 6, 8) are used which do not satisfy Grashof's condition $(4+8>5+6)$. Not a single link is fully rotating relative to the fixed link. These four-bars are referred to as *double-rockers of second kind*. Figure 17.5a shows the limit positions of both rockers. The angular range of each rocker is a single sector which is symmetrical to the base line. For a single input angle the two existing positions of the four-bar are shown (one of them with dashed lines). In Figs. 17.5a,b,c the four given lengths are given to different links of the four-bar. It is seen that depending on this distribution the fixed link is inside the angular range of either both rockers (Fig. 17.5a) or of a single rocker (Fig. 17.5b) or of no rocker (Fig. 17.5c).

Foldable Four-Bars Satisfying Grashof's Equality Condition $\ell_{\min}+\ell_{\max}=\ell'+\ell''$.

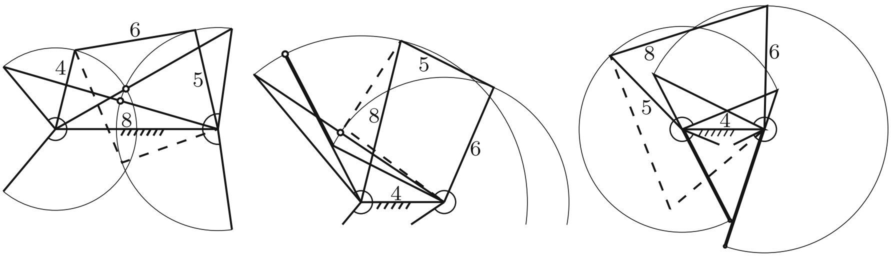

Fig. 17.5 Three double-rockers of second kind with different distributions of the link lengths (4, 5, 6, 8). No link is fully rotating

For demonstration the link lengths (1, 3, 4, 6) are used which satisfy the condition that $1+6=3+4$. Depending on whether the shortest link is the fixed link or the input link or the coupler the four-bar is either a double-crank or a crank-rocker or a double-rocker of first kind, respectively (compare Figs. 17.4a, b, c). In this respect there is no difference to the general case of four-bars satisfying the inequality condition $\ell_{\min}+\ell_{\max}<\ell'+\ell''$. The equality $\ell_{\min}+\ell_{\max}=\ell'+\ell''$ has the consequence that the four-bar is *foldable*. In a folded position all four links are collinear. Two different kinds of foldable four-bars have to be distinguished:

- first kind: $r_1+a\ =r_2+\ell$ (Fig. 17.6a)
- second kind: $r_1+r_2=a+\ell$ (Fig. 17.6b).

With link lengths (1, 3, 4, 6) the following foldable four-bars $(\ell,\, r_1,\, a,\, r_2)$ can be formed:
Foldable four-bars of first kind: Two double-cranks (1, 3, 4, 6), (1, 4, 3, 6);
four crank-rockers (4, 1, 6, 3), (3, 1, 6, 4), (6, 1, 4, 3), (6, 1, 3, 4);
two double-rockers of first kind (4, 6, 1, 3), (3, 6, 1, 4) ;
Foldable four-bars of second kind: One double-crank (1, 3, 6, 4);
two crank-rockers (3, 1, 4, 6), (4, 1, 3, 6);
one double-rocker of first kind (6, 4, 1, 3).

Example: The foldable four-bar of first kind in Fig. 17.6a is the double-rocker with $(\ell,\, r_1,\, a,\, r_2)=(4,6,1,3)$, and the foldable four-bar of second kind in Fig. 17.6b is the double-rocker with $(\ell,\, r_1,\, a,\, r_2)=(6,4,1,3)$. For a single angle φ of the input link the two associated positions of coupler and output link are shown. The points P_1 and P_2 are the instantaneous centers of rotation of the coupler in these positions. Let x be the coordinate of P_1 or P_2. In positions sufficiently close to the folded position ($\varphi=\psi=0$ in Fig. 17.6a and $\varphi=\pi-\psi=0$ in Fig. 17.6b) the following approximations are valid:

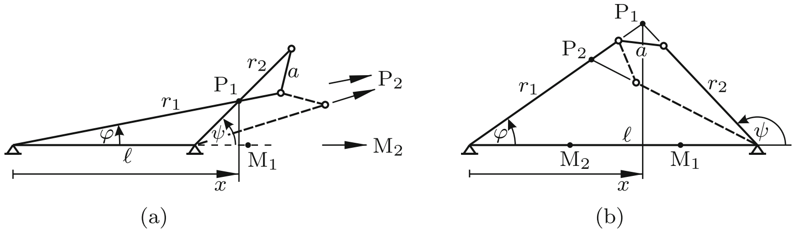

Fig. 17.6 **(a)** Foldable four-bar of first kind: $r_1+a=r_2+\ell$ ($\ell=4$, $r_1=6$, $a=1$, $r_2=3$). **(b)** Foldable four-bar of second kind: $r_1+r_2=a+\ell$ ($\ell=6$, $r_1=4$, $a=1$, $r_2=3$). Instantaneous centers of rotation P_1 and P_2 of the coupler tend toward M_1 and M_2 when the four-bar is folding

$$x\tan\varphi \approx \begin{cases} (x-\ell)\tan\psi & \text{(foldable four-bars of first kind)} \\ (\ell-x)\tan(\pi-\psi) & \text{(foldable four-bars of second kind).} \end{cases} \tag{17.5}$$

In Sect. 17.2 these approximations are used for determining instantaneous centers of rotation of the coupler in folded positions when intersection points P_1 and P_2 do not exist. End of example.

In the folded position motion is possible in two ways with either $\dot{\psi}/\dot{\varphi}>0$ or $\dot{\psi}/\dot{\varphi}<0$. In engineering applications of foldable four-bars provisions must be made either to avoid the folded position or to pass through it with prescribed sense of rotation.

Consider again Figs. 17.3a,b,c. When the input link of length r_1 is moving away from its limit position, the joint connecting coupler and output link is free to move in two different directions as is indicated by arrows. From this the following conclusion is drawn. Two positions of a four-bar which are associated with an arbitrarily given angle of a *rocker* can be reached one from the other by a continuous motion. The four-bars in Figs. 17.4a,c as well as those in Figs. 17.5a,b,c have this property. In contrast, two positions of a four-bar which are associated with an arbitrarily given angle of a *crank* cannot be reached one from the other by a continuous motion, but only by disconnection and reassembly (Figs. 17.4b,c). Exception: Foldable four-bars. Transition from one position to the other is possible via the folded position.

17.2 Transfer Function

From Figs. 17.5 and 17.4 it is known that to every position $(\varphi,\,\psi)$ of the four-bar the position symmetrical to the base line $\overline{A_0B_0}$ with angles $(-\varphi,\,-\psi)$ exists. This symmetry is found in all subsequent equations. The transfer function determines ψ as function of φ. First, implicit forms $f(\varphi,\psi)=0$ of the transfer function are formulated. Starting point are the coordinates of

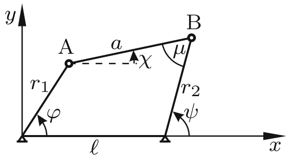

Fig. 17.7 Four-bar with input angle φ, output angle ψ, inclination angle χ of the coupler, transmission angle μ

the points A and B in the x, y-system shown in Fig. 17.7:

$$\left.\begin{aligned} x_{\mathrm{A}} &= r_1\cos\varphi\,, \qquad & x_{\mathrm{B}} &= \ell + r_2\cos\psi\,,\\ y_{\mathrm{A}} &= r_1\sin\varphi\,, \qquad & y_{\mathrm{B}} &= \qquad r_2\sin\psi\,. \end{aligned}\right\} \tag{17.6}$$

The constant length a of the coupler requires that $(x_{\mathrm{B}}-x_{\mathrm{A}})^2+(y_{\mathrm{B}}-y_{\mathrm{A}})^2 = a^2$ or explicitly

$$(\ell + r_2\cos\psi - r_1\cos\varphi)^2 + (r_2\sin\psi - r_1\sin\varphi)^2 - a^2 = 0\,. \tag{17.7}$$

This is already the desired equation $f(\varphi,\psi)=0$. Reformulation gives it the form

$$f = 2r_2(\ell - r_1\cos\varphi)\cos\psi - 2r_1r_2\sin\varphi\sin\psi - 2\ell r_1\cos\varphi + r_1^2 + \ell^2 + r_2^2 - a^2 = 0 \tag{17.8}$$

or alternatively

$$f = 2\ell r_2\cos\psi - 2\ell r_1\cos\varphi - 2r_1r_2\cos(\varphi-\psi) + r_1^2 + \ell^2 + r_2^2 - a^2 = 0\,. \tag{17.9}$$

Equation (17.8) has the form

$$A(\varphi)\cos\psi + B(\varphi)\sin\psi = C(\varphi) \tag{17.10}$$

with coefficients

$$A = 2r_2(\ell - r_1\cos\varphi),\quad B = -2r_1r_2\sin\varphi\,,\quad C = 2r_1\ell\cos\varphi - (r_1^2+\ell^2+r_2^2-a^2)\,. \tag{17.11}$$

For every angle φ there exist two solutions ψ_1 and ψ_2. They are determined through their sines and cosines:

$$\left.\begin{aligned} \cos\psi_k &= \frac{AC + (-1)^k B\sqrt{A^2+B^2-C^2}}{A^2+B^2}\,,\\ \sin\psi_k &= \frac{BC - (-1)^k A\sqrt{A^2+B^2-C^2}}{A^2+B^2} \end{aligned}\right\}\ (k=1,2)\,. \tag{17.12}$$

These expressions depend on three parameters only, namely, on r_1/ℓ, r_2/ℓ and a/ℓ. Equations (17.11) yield

$$A^2 + B^2 = 4r_2^2(\ell^2 + r_1^2 - 2r_1\ell\cos\varphi) = -4r_2^2(C + r_2^2 - a^2)\,, \tag{17.13}$$

$$\begin{aligned} A^2 + B^2 - C^2 &= 4r_2^2a^2 - (C + 2r_2^2)^2 \\ &= -[C + 2r_2(a + r_2)][C - 2r_2(a - r_2)] \qquad (17.14) \\ &= -[2r_1\ell\cos\varphi - (r_1^2 + \ell^2) + (r_2 + a)^2] \\ &\quad \times[2r_1\ell\cos\varphi - (r_1^2 + \ell^2) + (r_2 - a)^2]\,. \qquad (17.15) \end{aligned}$$

The angles ψ_1 and ψ_2 are real for all angles φ satisfying the condition $A^2 + B^2 - C^2 \ge 0$. Let ϕ denote all angles φ for which the equality sign is valid. From (17.15) the cosines of these angles are obtained:

$$\cos\phi_{1,2} = \frac{r_1^2 + \ell^2 - (r_2 \mp a)^2}{2r_1\ell}\,. \tag{17.16}$$

These are the Eqs.(17.1). The angles are the limit angles of the input link known from Figs. 17.3a,b,c .

This section is closed with an application of (17.9) to foldable four-bars (see Figs. 17.6a,b). In the process of folding the instantaneous centers of rotation P_1 and P_2 of the coupler tend toward points M_1 and M_2 on the base line. These points are determined by combining (17.5) and (17.9). First, foldable four-bars of first kind are considered. In the limit $\varphi \to 0$, $\psi \to 0$ (17.5) yields $x/(x - \ell) = \psi/\varphi$. With $\ell = r_1 - r_2 + a$ (17.9) becomes

$$r_1(r_1+a)+r_2(r_2-a)-r_1r_2[1+\cos(\varphi-\psi)]-(r_1-r_2+a)(r_1\cos\varphi-r_2\cos\psi) = 0\,. \tag{17.17}$$

Taylor expansion up to second-order terms and division through φ^2 produces for $\lambda = \psi/\varphi = x/(x - \ell)$ the quadratic equation $\lambda^2 r_2(r_2 - a) - 2r_1r_2\lambda = -r_1(r_1 + a)$. The solutions $\lambda_{1,2}$ and the associated coordinates $x_{1,2}$ of M_1 and M_2 are

$$\lambda_{1,2} = \frac{r_1r_2 \pm \sqrt{r_1r_2a\ell}}{r_2(r_2 - a)}\,, \qquad x_{1,2} = \frac{\lambda_{1,2}}{\lambda_{1,2} - 1}\,\ell\,. \tag{17.18}$$

The solution for foldable four-bars of second kind is obtained in a similar way. In (17.9) the substitutions $\psi = \pi - \alpha$ and $\ell = r_1 + r_2 - a$ are made. Following this, a Taylor expansion up to second-order terms is made. The result is a quadratic equation for $\lambda = \alpha/\varphi = x/(\ell - x)$. The solutions $\lambda_{1,2}$ are identical with those in (17.18):

$$\lambda_{1,2} = \frac{r_1r_2 \pm \sqrt{r_1r_2a\ell}}{r_2(r_2 - a)}\,, \qquad x_{1,2} = \frac{\lambda_{1,2}}{\lambda_{1,2} + 1}\,\ell\,. \tag{17.19}$$

Examples: The link lengths of Fig. 17.6a yield $x_1 \approx 5.17$, $x_2 \approx 10.8$ and those of Fig. 17.6b yield $x_1 \approx 4.64$, $x_2 \approx 2.21$. These are the points M_1 and M_2 shown in the figure. End of examples.

17.3 Interchange of Input Link and Fixed Link

In Fig. 17.8 the four-bar A_0ABB_0 with link lengths ℓ, r_1, a, r_2 is called four-bar F. Dashed lines parallel to the fixed link and to the input link define the point P. The quadrilateral B_0PAB is drawn one more time in dotted lines. The dotted quadrilateral is called four-bar F^*. Its fixed link has length r_1, and its input link has length ℓ. Both four-bars have the same coupler and the same output link. If F is a foldable four-bar, also F^* is foldable. If F is a double-rocker of first kind (of second kind), also F^* is a double-rocker of first kind (of second kind). If F is a double-crank, F^* is either a double-crank or a crank-rocker. If F is a crank-rocker, F^* is either a double-crank (if fixed link and crank are interchanged) or a crank-rocker (if fixed link and rocker are interchanged). Example: Let F be the crank-rocker in Fig. 17.4b. Interchange of fixed link and crank produces the double-crank of Fig. 17.4a.

In Fig. 17.8 F and F^* have one and the same input angle φ. The relation between the output angles ψ and ψ^* is seen to be

$$\psi + \psi^* \equiv \varphi + \pi \,. \tag{17.20}$$

For a given angle φ Eqs.(17.12) determine in the four-bar F two angles ψ_1 and ψ_2 and in the four-bar F^* with coefficients $A^* = 2r_2(r_1 - \ell\cos\varphi)$, $B^* = -2\ell r_2 \sin\varphi$, $C^* = C$ two angles ψ_1^* and ψ_2^*. The coordination of the pairs of angles is as follows: $\psi_1 + \psi_2^* \equiv \varphi + \pi$. This is verified by substituting

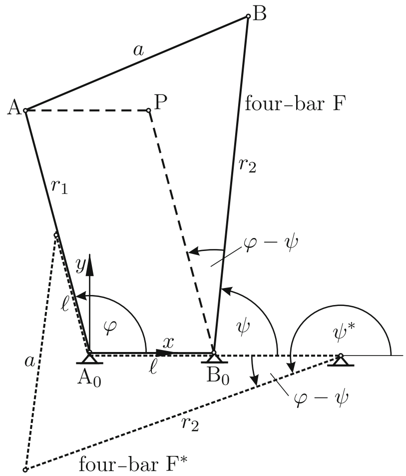

Fig. 17.8 Four-bar F and the associated four-bar F^* with link lengths r_1 and ℓ interchanged

A, B, C and A^*, B^*, C^* into the equation $\cos\psi_1\cos\psi_2^* - \sin\psi_1\sin\psi_2^* \equiv -\cos\varphi$.

17.4 Inclination Angle of the Coupler. Transmission Angle

Figure 17.7 defines the inclination angle χ of the coupler against the base line. Its dependency on φ is found by the same method that was used for ψ . Point B has coordinates $x_{\text{B}} = r_1\cos\varphi + a\cos\chi$ and $y_{\text{B}} = r_1\sin\varphi + a\sin\chi$. These expressions are substituted into the constraint equation $(x_{\text{B}} - \ell)^2 + y_{\text{B}}^2 = r_2^2$. This results in the equation

$$\bar{A}\cos\chi + \bar{B}\sin\chi = \bar{C}\ , \tag{17.21}$$

$$\bar{A} = -2a(\ell - r_1\cos\varphi)\ , \quad \bar{B} = 2r_1 a\sin\varphi\ , \quad \bar{C} = 2r_1\ell\cos\varphi - (r_1^2 + \ell^2 + a^2 - r_2^2)\ . \tag{17.22}$$

These coefficients are obtained from those in (17.11) by interchanging r_2 and $-a$. The equation has the solutions

$$\left.\begin{aligned} \cos\chi_k &= \frac{\bar{A}\bar{C} - (-1)^k\bar{B}\sqrt{\bar{A}^2 + \bar{B}^2 - \bar{C}^2}}{\bar{A}^2 + \bar{B}^2}\ , \\ \sin\chi_k &= \frac{\bar{B}\bar{C} + (-1)^k\bar{A}\sqrt{\bar{A}^2 + \bar{B}^2 - \bar{C}^2}}{\bar{A}^2 + \bar{B}^2} \end{aligned}\right\} (k = 1, 2). \tag{17.23}$$

The exponent k in this equation must be the same as in (17.12). Only then the constraint equation $r_1\cos\varphi + a\cos\chi = \ell + r_2\cos\psi$ is satisfied.

The angle χ reaches a stationary value (maximum or minimum) when the angular velocity $\dot{\chi}$ of the coupler is zero. This is the case when the instantaneous center of rotation P_{30} , i.e., the intersection of input link and output link, is at infinity. Figure 17.9 shows that this is possible in two positions. Let $\varphi = \varphi_\infty$ and χ_{stat} be the associated angles. One position is characterized by $\psi = \varphi_\infty$ and the other by $\psi = \varphi_\infty + \pi$. Equation (17.10) yields for $\cos\varphi_\infty$ the two expressions given below. Expressions for the associated stationary angles χ_{stat} are obtained from the cosine law applied to the triangles shown in Fig. 17.9:

$$\cos\varphi_\infty = \frac{\ell^2 - a^2 + (r_1 \mp r_2)^2}{2\ell(r_1 \mp r_2)}\ , \quad \cos\chi_{\text{stat}} = \frac{\ell^2 + a^2 - (r_1 \mp r_2)^2}{2a\ell}\ . \tag{17.24}$$

The angles φ_∞ have a kinematical interpretation. They determine the directions of asymptotes of the fixed centrode of the coupler. The centrode has no asymptotes if both cosines have absolute values > 1 , i.e., if the conditions $(\ell - a)^2 > (r_1 - r_2)^2$ and $(\ell + a)^2 < (r_1 + r_2)^2$ are satisfied. This is the

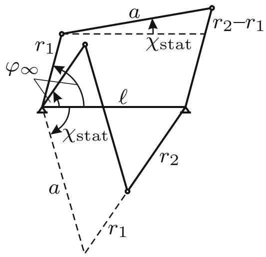

Fig. 17.9 Stationary values of the angle χ occur when the cranks are parallel

case if and only if the coupler is fully rotating. These four-bars are either double-cranks (Fig. 17.4a) or double-rockers of first kind (Fig. 17.4c). In Ex. 6 of Sect. 15.1.2 centrodes of couplers of four-bars with special link lengths were investigated.

In Fig. 17.7 the transmission angle μ of a four-bar is defined. Its dependency on φ is obtained as follows. The length of the diagonal starting from A is expressed by means of the cosine law once in terms of $\cos\varphi$ and once in terms of $\cos\mu$. The identity of these expressions results in

$$\cos\mu = \frac{2r_1\ell\cos\varphi - (r_1^2+\ell^2) + r_2^2 + a^2}{2r_2 a}\,. \tag{17.25}$$

Extremal values of μ are obtained from (17.1) by interchanging (r_1, ℓ) and (r_2, a):

$$\cos\mu_{\text{stat}} = \frac{r_2^2 + a^2 - (\ell \mp r_1)^2}{2r_2 a}\,. \tag{17.26}$$

In positions with these extremal values the input link and the fixed link are collinear (see Fig. 17.3). In phases of motion in which the coupler is required to transmit a large torque to the output link the transmission angle μ should differ from $\pi/2$ as little as possible. In other words: $|\cos\mu|$ should be as small as possible.

17.5 Transmission Ratio. Angular Acceleration of Output Link

The angular velocity ratio $i = \dot\varphi/\dot\psi$ is called *transmission ratio* of the four-bar. In what follows, the inverse value $1/i = \dot\psi/\dot\varphi$ is represented in geometric and in analytical form. The geometric form is obtained from (15.6). Let the fixed link, the input link and the output link be links 0, 1 and 2, respectively, so that $\omega_{10} = \dot\varphi$ and $\omega_{20} = \dot\psi$ (see Fig. 17.10). Equation (15.6) with $i = 2$, $j = 1$, $k = 0$ yields the expression

$$\frac{1}{i} = \frac{\dot\psi}{\dot\varphi} = \frac{\varrho_{P_{10}P_{12}}}{\varrho_{P_{20}P_{12}}} = \frac{x_{12}}{x_{12}-\ell} = \frac{\xi}{\xi-1} \qquad \left(\xi = \frac{x_{12}}{\ell}\right) . \tag{17.27}$$

Here, $x_{12}(\varphi)$ is the coordinate of the instantaneous center P_{12} along the base line. The dimensionless quantity ξ is zero at the center P_{10} and it equals one at the center P_{20}. Over the ξ-axis thus defined the ratio $1/i$ is plotted at the center P_{12}.

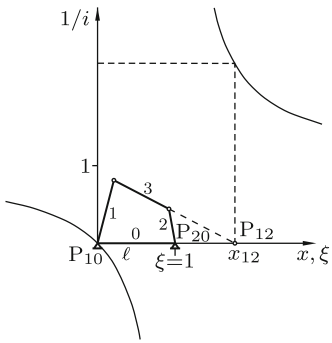

Fig. 17.10 Dimensionless coordinate $\xi = x_{12}/\ell$ of the instantaneous center P_{12} and inverse transmission ratio $1/i$ as function of ξ

An analytical expression for the ratio $1/i$ is found by differentiating the transfer function $f(\varphi,\psi) = 0$ with respect to time:

$$\dot\varphi\,\frac{\partial f}{\partial\varphi} + \dot\psi\,\frac{\partial f}{\partial\psi} = 0 . \tag{17.28}$$

Hence

$$\frac{1}{i} = \frac{\dot\psi}{\dot\varphi} = -\frac{\partial f}{\partial\varphi}\Big/\frac{\partial f}{\partial\psi} . \tag{17.29}$$

Equation (17.9) yields

$$\frac{\partial f}{\partial\varphi} = 2\ell r_1\sin\varphi + 2r_1r_2\sin(\varphi-\psi) , \qquad \frac{\partial f}{\partial\psi} = -2\ell r_2\sin\psi - 2r_1r_2\sin(\varphi-\psi) . \tag{17.30}$$

Hence

$$\frac{1}{i} = \frac{r_1}{r_2}\,\frac{\ell\sin\varphi + r_2\sin(\varphi-\psi)}{\ell\sin\psi + r_1\sin(\varphi-\psi)} = \frac{r_1}{r_2}\,\frac{\ell\sin\varphi + r_2(\sin\varphi\cos\psi - \cos\varphi\sin\psi)}{\ell\sin\psi + r_1(\sin\varphi\cos\psi - \cos\varphi\sin\psi)} . \tag{17.31}$$

Temporarily, this is abbreviated as $r_1N/(r_2D)$ (numerator N, denominator D). Equations (17.12) yield the expressions

$$N(A^2+B^2)=\ell(A^2+B^2)\sin\varphi+r_2\Big[(A\sin\varphi-B\cos\varphi)C \\ \mp(B\sin\varphi+A\cos\varphi)\sqrt{A^2+B^2-C^2}\,\Big]\,, \tag{17.32}$$

$$D(A^2+B^2)=\ell\Big(BC\pm A\sqrt{A^2+B^2-C^2}\,\Big)+r_1\Big[(A\sin\varphi-B\cos\varphi)C \\ \mp(B\sin\varphi+A\cos\varphi)\sqrt{A^2+B^2-C^2}\,\Big]\,. \tag{17.33}$$

From (17.11) it follows that

$$\left.\begin{aligned} &A\sin\varphi-B\cos\varphi=2r_2\ell\sin\varphi\,,\\ &B\sin\varphi+A\cos\varphi=2r_2(\ell\cos\varphi-r_1)\,,\\ &\ell B+r_1(A\sin\varphi-B\cos\varphi)=0\,. \end{aligned}\right\} \tag{17.34}$$

These equations in combination with (17.13) and (17.14) yield the formula

$$\frac{2}{i}=\frac{\cos\varphi-p_1}{\cos\varphi-p_2}\pm\frac{(\cos\varphi-p_3)\sin\varphi}{(\cos\varphi-p_2)\sqrt{\lambda^2-(\cos\varphi-p_4)^2}} \tag{17.35}$$

with dimensionless constants

$$\left.\begin{aligned} &\lambda=\frac{r_2a}{r_1\ell}\,,\qquad p_1=\frac{r_1}{\ell}\,,\qquad p_2=\frac{r_1^2+\ell^2}{2r_1\ell}=\frac{1}{2}\Big(p_1+\frac{1}{p_1}\Big)\geq 1\,,\\ &p_3=p_2-\frac{r_2^2-a^2}{2r_1\ell}\,,\qquad p_4=p_2-\frac{r_2^2+a^2}{2r_1\ell}\,. \end{aligned}\right\} \tag{17.36}$$

These constants are related as follows:

$$p_2^2-1=(p_1-p_2)^2\,,\qquad (p_4-p_2)^2-\lambda^2=(p_3-p_2)^2\,. \tag{17.37}$$

The expression $\cos\varphi-p_2$ in (17.35) is zero only if the conditions $\varphi=0$ and $r_1=\ell$ are satisfied which imply that also $r_2=a$. The square root in (17.35) is zero for angles $\varphi=\phi_{1,2}$ satisfying one of the equations $\cos\phi_{1,2}-p_4=\pm\lambda$. This is Eq.(17.1) defining the angles shown in Figs. 17.3a,b,c .

With the exception of p_1 all constants in (17.36) are invariant with respect to an interchange of base length ℓ and input link length r_1. Because of the first Eq.(17.37) this is true also for $(p_1-p_2)^2$. A relation between the ratios $1/i$ and $1/i^*$ of the two four-bars with interchanged link lengths is obtained by differentiating the identity Eq.(17.20) with respect to time:

$$\frac{1}{i}+\frac{1}{i^*}=\frac{\dot\psi}{\dot\varphi}+\frac{\dot\psi^*}{\dot\varphi}\equiv 1\,. \tag{17.38}$$

The total time derivative of (17.28) yields the transfer characteristics on the acceleration level:

$$\ddot{\varphi}\,\frac{\partial f}{\partial\varphi}+\ddot{\psi}\,\frac{\partial f}{\partial\psi}+\dot{\varphi}^2\,\frac{\partial^2 f}{\partial\varphi^2}+2\dot{\varphi}\dot{\psi}\,\frac{\partial^2 f}{\partial\varphi\partial\psi}+\dot{\psi}^2\,\frac{\partial^2 f}{\partial\psi^2}=0\,. \tag{17.39}$$

Furthermore, $\dot{\psi}=\dot{\varphi}/i$ with (17.29) for $1/i$. This together with the derivatives in (17.30) yields for $\ddot{\psi}$ the expression

$$\ddot{\psi}=i\ddot{\varphi}+\dot{\varphi}^2\,\frac{r_1\ell\cos\varphi-(r_2\ell/i^2)\cos\psi+r_1r_2(1-1/i)^2\cos(\varphi-\psi)}{r_2\ell\sin\psi+r_1r_2\sin(\varphi-\psi)}\,. \tag{17.40}$$

17.6 Stationary Values of the Transmission Ratio

In this section geometrical and analytical methods are used for determining those input angles φ for which the ratio $1/i$ in (17.35) and hence the transmission ratio i itself attains stationary values. Starting from Fig. 17.10 Freudenstein [14] discovered the following geometrical relationship. Imagine that the input link is moving with $\dot{\varphi}>0$ through its entire angular range. In the course of this motion the instantaneous center P_{12} moves along the ξ-axis. Whenever it has zero velocity, the ratio $1/i$ attains a stationary value. This is a consequence of the monotonicity property of the function $1/i(\xi)$ shown in the figure. The velocity of P_{12} is zero if and only if the coupler-fixed point momentarily coinciding with P_{12} has a velocity in the direction of the coupler (labeled body 3). Then the center P_{30} of the coupler lies on the normal to the coupler erected in P_{12}. In other words: In positions of the four-bar with a stationary value of $1/i$ the lines $\overline{P_{12}P_{30}}$ and $\overline{P_{31}P_{32}}$ are mutually orthogonal[2]. Figure 17.11 shows two different four-bars in such positions.

If a stationary value occurs at $\varphi=0$ or at $\varphi=\pi$, P_{12} and P_{30} are located on the base line, and the coupler is orthogonal to the base line. Then the parameters satisfy the condition

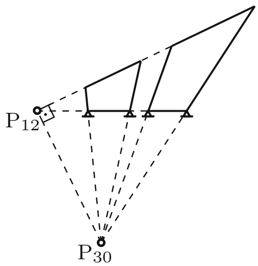

Fig. 17.11 Two four-bars in positions when $\overline{P_{12}P_{30}}$ is orthogonal to the coupler

[2] In Bobillier's Theorem 15.6 the line $\overline{P_{12}P_{30}}$ was shown to play another important role (line h in Fig. 15.19)

$$\left.\begin{array}{ll}\text{stationary value at } \varphi=0: & (\ell-r_1)^2+a^2=r_2^2\,,\\ \text{stationary value at } \varphi=\pi: & (\ell+r_1)^2+a^2=r_2^2\,.\end{array}\right\} \tag{17.41}$$

In the vicinity of an angle φ for which $1/i$ has a stationary value the angle between the lines $\overline{P_{12}P_{30}}$ and $\overline{P_{31}P_{32}}$ is very sensitive to changes of φ. The desired angle φ can, therefore, be determined graphically rather precisely by checking the orthogonality. In order to determine for a given four-bar all positions with a stationary value of $1/i$ the four-bar and the center P_{12} must be drawn for a number of (monotonically increasing) angles φ over the entire possible range $\phi_1 \le \varphi \le \phi_2$. A stationary value of $1/i$ is passed every time the moving center P_{12} changes its sense of direction along the ξ-axis (jumps from ∞ to $-\infty$ do not count as changes of sense of direction). Once a position is known approximately it can be improved by checking the angle between the lines $\overline{P_{12}P_{30}}$ and $\overline{P_{31}P_{32}}$.

Example: For the double-crank in Fig. 17.4a this investigation reveals that stationary values of $1/i$ occur in the two positions shown in Fig. 17.12a with $\varphi \approx 9^\circ$ and with $\varphi \approx 95^\circ$. With the coordinate of P_{12} (17.27) yields for the position $\varphi \approx 9^\circ$ a maximum $(1/i)_{\max} \approx 2.7$ and for the position $\varphi \approx 95^\circ$ a minimum $(1/i)_{\min} \approx 0.42$.

For the crank-rocker of Fig. 17.4b the same investigation can be made. This is unnecessary, however, because this four-bar is obtained from the previously investigated one by interchanging the fixed link and the input link. From (17.38) it follows that two four-bars thus related have stationary values of $1/i$ for one and the same angles φ. Furthermore, these stationary values add up to one. If the stationary value is a maximum in one of the four-bars, it is a minimum in the other and vice versa. Hence the crank-rocker of Fig. 17.4b has at $\varphi \approx 9^\circ$ a minimum $(1/i)_{\min} \approx -1.7$ and at $\varphi \approx 95^\circ$ a maximum $(1/i)_{\max} \approx 0.58$. Figure 17.12b shows the crank-rocker in these positions. End of example.

In what follows, two analytical methods for determining stationary values of $1/i$ are described. Method 1 is a direct method based on (17.35). With the abbreviation $x = \cos\varphi$ it is written in the form

$$\left.\begin{array}{l}\dfrac{2}{i(x)} = \dfrac{x-p_1}{x-p_2} \pm \dfrac{(x-p_3)Q}{(x-p_2)P}\,,\\ P=\sqrt{\lambda^2-(x-p_4)^2}\,, \qquad Q=\sqrt{1-x^2}\,.\end{array}\right\} \tag{17.42}$$

The stationarity condition $\mathrm{d}(1/i)/\mathrm{d}x = 0$ has the form (the prime denotes the derivative with respect to x)

$$\mp(p_1-p_2)P^2 = (p_3-p_2)PQ + (x-p_2)(x-p_3)(PQ'-QP')\,. \tag{17.43}$$

Now, $P' = -(x-p_4)/P$ and $Q' = -x/Q$ are substituted. The resulting equation is multiplied by PQ. This eliminates the case $\sin\varphi = 0$. Whether

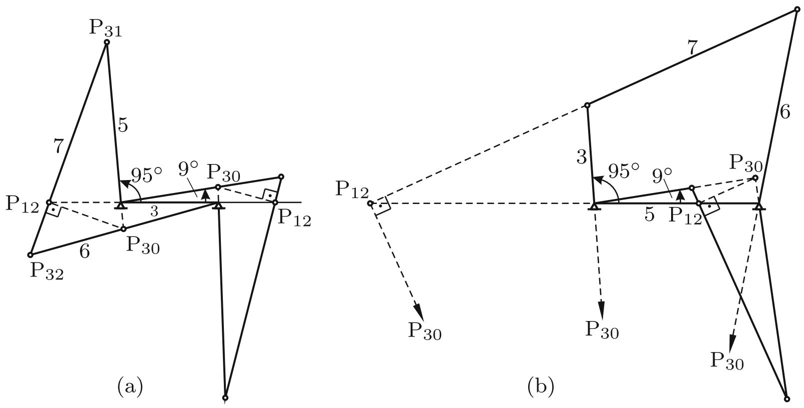

Fig. 17.12 The double-crank of Fig. 17.4a **(a)** and the crank-rocker of Fig. 17.4b **(b)** in the two positions with stationary values of $1/i$

this is a solution is checked with (17.41). After this multiplication the equation has the form

$$\begin{aligned}&\pm (p_1-p_2)[(x-p_4)^2-\lambda^2]\sqrt{(x^2-1)[(x-p_4)^2-\lambda^2]}\\&=(p_3-p_2)(x^2-1)[(x-p_4)^2-\lambda^2]\\&\quad-(x-p_2)(x-p_3)[p_4(1+x^2)+x(\lambda^2-p_4^2-1)]\,.\end{aligned}\tag{17.44}$$

The special case $r_1=\ell$ is characterized by $p_1=p_2=1$ and, therefore, by the third-order equation

$$(p_3-1)(1+x)[\lambda^2-(x-p_4)^2]+(x-p_3)[p_4(1+x^2)+x(\lambda^2-p_4^2-1)]=0\,.\tag{17.45}$$

The equation is quadratic if, in addition, also $a=\ell$.

In the general case $r_1\neq\ell$, (17.44) is squared. The squared equation is invariant with respect to the interchange of r_1 and ℓ (see the comments following (17.36) and (17.37)). Because of the sign $\pm$ no extraneous roots are introduced by squaring. Equation (17.44) with the positive sign has the meaningless root $x=p_2>1$. This is verified with the help of (17.37). From this it follows that the squared equation is divisible by $(x-p_2)^2$. Following this division it is a sixth-order equation. The division is performed in two steps. Squaring results in the equation

$$\begin{aligned}&(\ x^2-1)[(x-p_4)^2-\lambda^2]^2\Big\{(p_1-p_2)^2[(x-p_4)^2-\lambda^2]-(p_3-p_2)^2(x^2-1)\Big\}\\&=(x-p_2)F(x)\Big\{(x-p_2)F(x)-2(p_3-p_2)(x^2-1)[(x-p_4)^2-\lambda^2]\Big\}\end{aligned}\tag{17.46}$$

with the third-order polynomial

$$F(x) = (x - p_3)[p_4(1 + x^2) + x(\lambda^2 - p_4^2 - 1)] \; . \qquad (17.47)$$

Taking into account (17.37) the expression in curled brackets on the left-hand side is written in the form $(x - p_2)(Ax + B)$ with constants

$$A = (p_1 - p_2)^2 - (p_3 - p_2)^2 \; , \qquad B = p_2 A - 2p_4(p_1 - p_2)^2 \; . \qquad (17.48)$$

Division of (17.46) by $(x - p_2)$ produces the equation

$$(x^2 - 1)[(x - p_4)^2 - \lambda^2]\Big\{[(x - p_4)^2 - \lambda^2](Ax + B) + 2(p_3 - p_2)F(x)\Big\}$$
$$= (x - p_2)[F(x)]^2 \; . \qquad (17.49)$$

The expression in curled brackets is a third-order polynomial $K_3x^3 + K_2x^2 + K_1x + K_0$ with coefficients

$$\left.\begin{aligned} K_3 &= A + 2p_4(p_3 - p_2) \; , \\ K_2 &= B - 2p_4A + 2(p_3 - p_2)(\lambda^2 - p_4^2 - 1 - p_3p_4) \; , \\ K_1 &= -2p_4B + A(p_4^2 - \lambda^2) + 2(p_3 - p_2)[p_4 - p_3(\lambda^2 - p_4^2 - 1)] \; . \end{aligned}\right\} \qquad (17.50)$$

Division by $(x - p_2)$ produces the second-order polynomial $K_3x^2 + (x + p_2)(K_2 + p_2K_3) + K_1$. With this expression (17.49) yields the desired sixth-order equation

$$(x^2-1)[(x-p_4)^2-\lambda^2][K_3x^2+(x+p_2)(K_2+p_2K_3)+K_1]-[F(x)]^2 = 0 \; . \qquad (17.51)$$

The coefficient of x^6 is

$$K_3 - p_4^2 = (p_1 - p_2)^2 - (p_3 - p_2 - p_4)^2 = \frac{(\ell^2 - a^2)(a^2 - r_1^2)}{(r_1\ell)^2} \; . \qquad (17.52)$$

The equation is of fifth order if $a = \ell$ and/or $a = r_1$. Only real roots $|x| \le 1$ are significant. For every such root it is checked to which sign in (17.44) the root belongs. With the same sign (17.42) and (17.12) determine the corresponding stationary value of $1/i$ and the angle ψ.

Example: With the parameters of the double-crank in Fig. 17.4a as well as with those of the crank-rocker in Fig. 17.4b (17.51) has the four real roots $x = \cos\varphi \approx -0.084$, 0.9882, 1.11 and 4.02. The first two roots determine the angles $\varphi \approx 94.8^\circ$ and $\varphi \approx 8.8^\circ$, respectively. These are the angles shown in Figs. 17.12a and b. End of example.

The second (historically the first) analytical method for determining stationary values of $1/i$ is due to Freudenstein [14]. Also this method leads to a sixth-order equation. The method starts out from Fig. 17.10 and from the coupler curve traced by a point C fixed on the coupler line $\overline{P_{31}P_{32}}$. Let $\eta =$ const be the coordinate of this point along the coupler line ($\eta = 0$, when

C is at P_{31} and $\eta > 0$, when C and P_{32} are on the same side of P_{31}). In Sect. 17.8.3 the equation of the coupler curve in the x, y-system of Fig. 17.7 is given. In what follows, only the coordinates of the intersection points of the curve with the x-axis are needed. They are the roots of Eq.(17.100) which is cubic with respect to x and to η:

$$(\eta - a)(x - \ell)(x^2 + \eta^2 - r_1^2) - \eta x[(x - \ell)^2 + (\eta - a)^2 - r_2^2] = 0\,. \quad (17.53)$$

The corresponding angle φ is determined by the cosine law:

$$\cos\varphi = \frac{x^2 + r_1^2 - \eta^2}{2r_1 x}\,. \quad (17.54)$$

In Sect. 17.8.4 it is pointed out that not every real root x of (17.53) represents an intersection point of the coupler-curve with the x-axis. A root represents a singular point without kinematical significance if it is associated with values $|\cos\varphi| > 1$. In what follows, only those roots are of interest which yield values $|\cos\varphi| \le 1$.

Let now C be the coupler-fixed point which coincides with P_{12} when the four-bar is in a position with a stationary value of $1/i$. In Fig. 17.13 this situation is shown. The coordinate η of this point is associated with a solution x of (17.53) which is equal to the stationary value of the coordinate x_{12} of the center P_{12}. Although x_{12} and x have different definitions, x as function of η has the same stationary value. From this it follows that the implicit derivative of (17.53) with respect to η is valid with $\mathrm{d}x/\mathrm{d}\eta = 0$. This is the equation

$$(x - \ell)(x^2 + \eta^2 - r_1^2) - x[(x - \ell)^2 + (\eta - a)^2 - r_2^2] - 2\ell\eta(\eta - a) = 0\,. \quad (17.55)$$

This equation and (17.53) together determine the unknowns x and η. De-

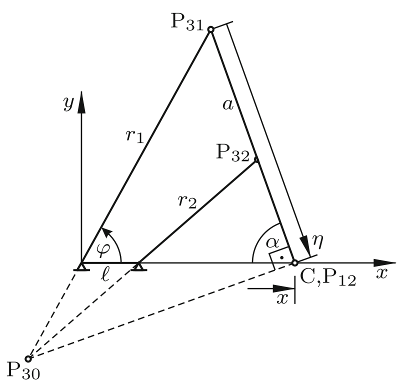

Fig. 17.13 Four-bar in a position with stationary value of $1/i$. The coupler point C momentarily coinciding with P_{12} has coordinates x and η

coupling leads to the desired sixth-order equation. This decoupling is achieved in several steps. First, (17.55) is multiplied by η and then (17.53) is subtracted. This results in the equation

$$a(x-\ell)(x^2+\eta^2-r_1^2)-2\ell\eta^2(\eta-a)=0\,. \tag{17.56}$$

This equation and (17.55) are rewritten by introducing the dimensionless variable $\xi=x/\ell$ already known and the new dimensionless variable $\nu=\eta/a$. The new equations for the unknowns ξ and ν are

$$\ell^2\xi^2-\xi(\ell^2+a^2+r_1^2-r_2^2)+r_1^2+a^2[-3\nu^2+2\nu(1+\xi)]=0\,, \tag{17.57}$$
$$\ell^2(\xi^3-\xi^2)+r_1^2(1-\xi)+a^2[-2\nu^3+\nu^2(1+\xi)]=0\,. \tag{17.58}$$

In order to get a linear equation for ν (17.57) is multiplied by $(\lambda_1+\lambda_2\nu)$ and then added to (17.58). The free coefficients λ_1 and λ_2 are then determined such that the coefficients of ν^3 and ν^2 equal zero. This yields two linear equations for λ_1 and λ_2. Their solutions are $\lambda_1=-(1+\xi)/9$, $\lambda_2=-2/3$. The resulting linear equation for ν has the solution

$$\nu=\frac{8(\ell^2\xi^3+r_1^2)+\xi^2(r_1^2-9\ell^2+a^2-r_2^2)+\xi(\ell^2-9r_1^2+a^2-r_2^2)}{2\big\{\xi^2(a^2+3\ell^2)-\xi[3(\ell^2+r_1^2-r_2^2)+a^2]+a^2+3r_1^2\big\}}\,. \tag{17.59}$$

This expression is substituted back into (17.57). The result of this procedure is the desired sixth-order equation for ξ:

$$C_6\xi^6+C_5\xi^5+C_4\xi^4+C_3\xi^3+C_2\xi^2+C_1\xi+C_0=0\,. \tag{17.60}$$

The coefficients[3] are

$$\left.\begin{aligned}
C_6&=4\ell^2(\ell^2-a^2)^2\,,\\
C_5&=4\ell^2[(r_2^2-r_1^2)(3\ell^2+5a^2)-3(\ell^2-a^2)^2]\,,\\
C_4&=(a^2+12\ell^2)[(\ell^2-a^2)^2+(r_1^2-r_2^2)^2-2\ell^2(r_1^2+r_2^2)]\\
&\quad-2a^4(r_1^2+r_2^2)+20\ell^2[3r_1^2(\ell^2+a^2)+a^2(r_1^2-r_2^2)]\,,\\
C_3&=-2\Big[2(\ell^6+r_1^6)+18\ell^2r_1^2(\ell^2+r_1^2)-3(\ell^4+r_1^4)(a^2+2r_2^2)\\
&\qquad+2\ell^2r_1^2(29a^2-12r_2^2)+2r_2^2(\ell^2+r_1^2)(3r_2^2-a^2)\\
&\qquad+(a^2-2r_2^2)(a^2-r_2^2)^2\Big]\,.
\end{aligned}\right\} \tag{17.61}$$

C_0, C_1 and C_2 are obtained from C_6, C_5 and C_4, respectively, by interchanging ℓ and r_1, and C_3 is symmetric with respect to ℓ and r_1. To every real solution ξ the corresponding ν is calculated from (17.59). With

[3] In [14] the symmetry with respect to ℓ and r_1 is not shown. The coefficient of x^5 is misprinted. The correct coefficient is $d[32b^2(a^2-c^2)-12(d^2-b^2)n]$. Another misprint occurs in Eq.(30) which must begin with $(x-d)$ instead of with $(x-d)^2$

$x = \ell\xi$ and $\eta = a\nu$ (17.54) determines the corresponding angle φ. The corresponding stationary value of $1/i$ is given by (17.27): $1/i = \xi/(\xi - 1)$.

Consider again two four-bars resulting one from the other by interchanging the link lengths r_1 and ℓ. Let (17.60) be the conditional equation for one of these four-bars. The equation for the other four-bar is $C_0\xi^6 + C_1\xi^5 + C_2\xi^4 + C_3\xi^3 + C_4\xi^2 + C_5\xi + C_6 = 0$. If ξ is a root of one equation, $1/\xi$ is root of the other equation. With both roots (17.59) and (17.54) determine one and the same angle φ. For both roots the corresponding quantities $1/i$ are calculated from (17.27). These two quantities add up to one.

It is seen that $C_6 = 0$ if $a = \ell$ and that $C_0 = 0$ if $a = r_1$. In either case (17.60) is of fifth order. Under the same conditions also the previous method resulted in a fifth-order equation (see (17.52)). In the case $r_1 = \ell$, the previous method resulted in the third-order Eq.(17.45). With the present method this case yields the identities $C_6 = C_0$, $C_5 = C_1$ and $C_4 = C_2$. Equation (17.60) then has the form

$$C_0\xi^6 + C_1\xi^5 + C_2\xi^4 + C_3\xi^3 + C_2\xi^2 + C_1\xi + C_0 = 0 \, . \tag{17.62}$$

If ξ is a root, also $1/\xi$ is a root. Also the quadratic equation $\xi^2 + b\xi + 1 = 0$ has this property. Hence there exist coefficients b_1 , b_2 , b_3 such that (17.62) has the form

$$C_0(\xi^2 + b_1\xi + 1)(\xi^2 + b_2\xi + 1)(\xi^2 + b_3\xi + 1) = 0 \, . \tag{17.63}$$

The determination of b_1 , b_2 , b_3 by comparison of coefficients requires solving a cubic equation.

17.7 Transmission of Forces and Torques

Transmission of motion is not the only purpose of mechanisms. Equally important is transmission of forces and torques. In what follows, the state of equilibrium of an arbitrary planar or spatial single-degree-of-freedom mechanism is investigated. The planar four-bar is just an example. For every mechanism the input variable is called φ, and the output variable is called ψ. Let, furthermore, M_1 be the driving torque applied to the input link, and let M_2 be the counteracting torque applied to the output link. Thus, a torque $M_1 > 0$ is accelerating the mechanism and a torque $M_2 > 0$ is decelerating it. In a state of equilibrium the ratio M_2/M_1 has a certain value. It is determined from the equilibrium condition. According to the principle of virtual power this is the equation

$$M_1\delta\dot{\varphi} + (-M_2)\delta\dot{\psi} = 0 \, . \tag{17.64}$$

From the definition of the transmission ratio $i = \dot{\varphi}/\dot{\psi}$ it follows that $\delta\dot{\psi} = \delta\dot{\varphi}/i$. Therefore, the equilibrium condition is $(M_1 - M_2/i)\delta\dot{\varphi} = 0$. Hence

$$\frac{M_2}{M_1} = i \ . \tag{17.65}$$

This equation is valid in the more general sense that φ and ψ are generalized coordinates (for example, angles or cartesian coordinates), and that M_1 , M_2 are the associated generalized forces (torques or forces).

In a mechanism for the generation of large forces or torques the transmission ratio i should be as large as possible. Typical examples are shears, prongs and clamping devices of various kinds. In what follows, the shears shown in Figs. 17.14a – d are investigated. Each of them is a four-bar. The input and output variables are the opening widths x_1 and x_2 between the points of application of the hand forces F_1 and the cutting forces F_2 , respectively. In each case the equilibrium condition (17.65) is

$$\frac{F_2}{F_1} = \frac{\dot{x}_1}{\dot{x}_2} \ . \tag{17.66}$$

In each case the ratio of forces is to be expressed in terms of the lengths given in the figures.
Solution: Since x_1 and x_2 describe relative positions, it is unnecessary to declare any particular link as fixed link. In Table 17.1 the velocities $\dot{x}_1$ and $\dot{x}_2$ are expressed in terms of relative angular velocities (positive counterclockwise). These expressions are obvious from the figures. In each expression

Table 17.1 Ratio F_2/F_1 in terms of angular velocities

shears	(a)	(b)	(c)	(d)
$\frac{F_2}{F_1} = \frac{\dot{x}_1}{\dot{x}_2}$	$\frac{\ell_1}{\ell_4}\,\frac{\omega_{10}}{\omega_{23}}$	$\frac{\ell_1+\ell_2}{\ell_4}\,\frac{\omega_{10}}{\omega_{20}}$	$\frac{\ell_1+\ell_2}{\ell_2+\ell_3+\ell_4}\,\frac{\omega_{10}}{\omega_{23}}$	$\frac{\ell_1}{\ell_4}\,\frac{\omega_{10}}{\omega_{23}}$

the two relative angular velocities are related through a constraint equation. These equations have the following forms.
(a) $\dot{x}_3 = -\ell_2\omega_{10} = -\ell_3\omega_{23}$,
(b) The constraint $\dot{x}_3 = 0$ means that $\ell_2\omega_{10} - (\ell_2 + \ell_3)\omega_{20} = 0$,
(c) $\dot{x}_3 = -\ell_3\omega_{10} = -(\ell_2 + \ell_3)\omega_{23}$,
(d) In Fig. 17.14d instantaneous centers are shown. From (15.6) it follows that $\omega_{10}/\omega_{30} = L_4/L_3$ and $\omega_{23}/\omega_{30} = L_1/L_2$ and, consequently, $\omega_{10}/\omega_{23} = L_2L_4/(L_1L_3)$.
With these constraint equations the final results shown in Table 17.2 are obtained.

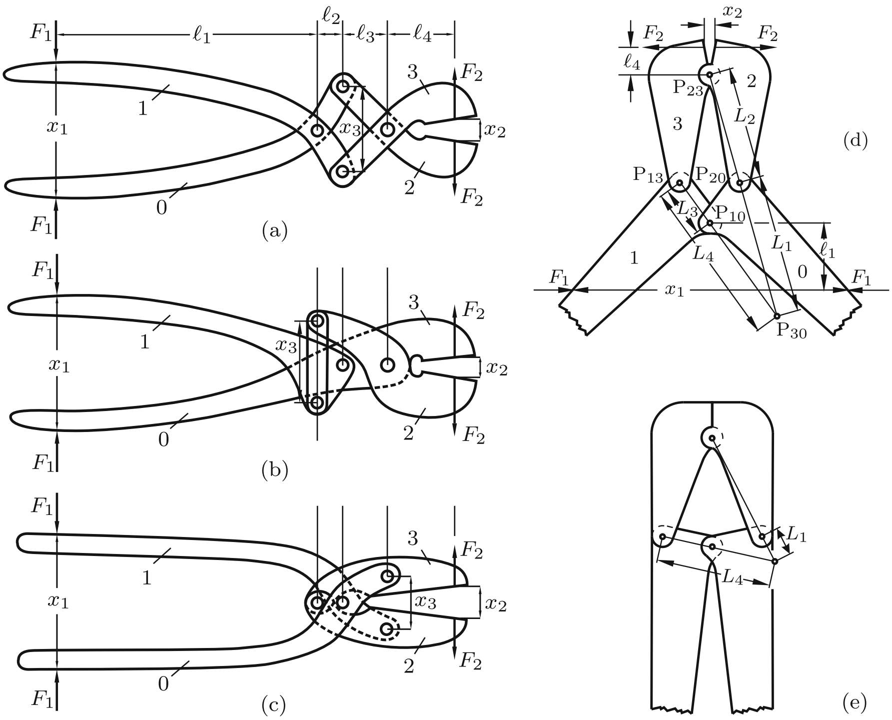

Fig. 17.14 Shears (**a**), (**b**), (**c**) with parameters $\ell_1, \ldots, \ell_4$ and shears (**d**) with instantaneous centers of rotation open and closed (**e**)

Table 17.2 Ratio F_2/F_1 in terms of link lengths

shears	(a)	(b)	(c)	(d)
$\dfrac{F_2}{F_1}$	$\dfrac{\ell_1\ell_3}{\ell_2\ell_4}$	$\dfrac{(\ell_1+\ell_2)(\ell_2+\ell_3)}{\ell_2\ell_4}$	$\dfrac{(\ell_1+\ell_2)(\ell_2+\ell_3)}{\ell_3(\ell_2+\ell_3+\ell_4)}$	$\dfrac{\ell_1 L_2}{\ell_4 L_3}\,\dfrac{L_4}{L_1}$

Comparative evaluation: Figures 17.14a,b,c are drawn with identical lengths $\ell_1 = 35$, $\ell_2 = 3.5$, $\ell_3 = 6$, $\ell_4 = 9$. With these lengths $F_2/F_1 \approx 6.7$ for the shears (a), $F_2/F_1 \approx 11.6$ for the shears (b) and $F_2/F_1 \approx 3.3$ for the shears (c). Shears (c) are the only ones in which the object to be cut can be placed in the position $\ell_4 = 0$. Then, $F_2/F_1 \approx 6.4$. With parameters of commercially available pruning-shears of this kind a ratio $F_2/F_1 = 15$ is possible. Compared with all other devices these shears have the advantage that for a given width of the object to be cut the opening angle between the shearing blades is the smallest.

In shears (d) the lengths L_2 and L_3 are constant. The lengths L_4 and L_1 depend very much on the opening angle. Both of them decrease monotonically in the process of closing the blades. Figure 17.14e shows the blades fully closed. The dimensions should be chosen such that in this position the instantaneous centers P_{13}, P_{10} and P_{20} are almost collinear as shown. In this case, the ratio L_4/L_1 is > 1 in every position, and it increases monotonically when the blades are closing. With shears of this kind reinforcement steel rods of 15 mm diameter can be cut by hand.

17.8 Coupler Curves

Every point fixed in the plane of the coupler traces a *coupler curve* when the four-bar is moving through its entire range. It is the complexity of these curves to which the four-bar owes much of its importance in engineering (see Fig. 17.2). In the following sections properties of coupler curves are investigated. The curvature of coupler curves was the subject of Sect. 15.3.3 (see Fig. 15.19).

17.8.1 Roberts/Tschebychev Theorem. Cognate Four-Bars

Figure 17.15 is started by drawing the four-bar $\mathrm{A}_0\mathrm{A}_1\mathrm{B}_1\mathrm{B}_0$ and a point C fixed in the plane of the coupler $\mathrm{A}_1\mathrm{B}_1$. This plane is represented by the *coupler triangle* (A_1,B_1,C). Subject of investigation is the coupler curve generated by C. To this basic figure lines $\mathrm{A}_0\mathrm{A}_2\mathrm{C}$ and $\mathrm{B}_0\mathrm{A}_3\mathrm{C}$ are added thus creating two parallelograms. In the next step, triangles similar to the coupler triangle are drawn as shown with bases $\mathrm{A}_2\mathrm{C}$ and $\mathrm{A}_3\mathrm{C}$. This results in points B_2 and B_3. Finally, another parallelogram defining the point C_0 is drawn. Point A_0 is made the origin of a complex plane. In this complex plane arbitrary points such as B_1, for example, are interpreted as complex numbers. The number is given the name of the point itself. For the addition of complex numbers the parallelogram rule is valid. This means, for example, that the number C_0 is the sum

$$C_0 = A_2 + (B_2 - A_2) + (C_0 - B_2)\ . \tag{17.67}$$

The coupler triangle (A_1,B_1,C) defines the complex number

$$z = \frac{|C - A_1|}{|B_1 - A_1|}\ \mathrm{e}^{\mathrm{i}\,\alpha}\ . \tag{17.68}$$

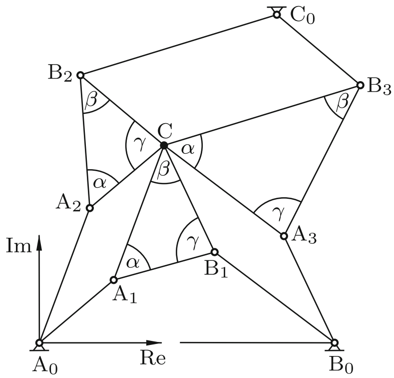

Fig. 17.15 Roberts/Tschebychev theorem

The definition is such that

$$C - A_1 = (B_1 - A_1)z \; . \tag{17.69}$$

For the three terms in (17.67) the figure yields the expressions

$$A_2 = C - A_1 = (B_1 - A_1)z \; , \qquad B_2 - A_2 = (C - A_2)z = A_1 z \; , \tag{17.70}$$

$$C_0 - B_2 = B_3 - C = (A_3 - C)z = (B_0 - B_1)z \; . \tag{17.71}$$

Substitution into (17.67) reveals that

$$C_0 = (B_1 - A_1 + A_1 + B_0 - B_1)z = B_0 z = \text{ const} \; . \tag{17.72}$$

Thus, C_0 remains fixed independent of the motion of the four-bar $A_0A_1B_1B_0$. From this follows

Theorem 17.2. (Roberts[4]/Tschebychev[5]) *For every four-bar* $A_0A_1B_1B_0$ *with a coupler point* C *there exist two additional four-bars* $A_0A_2B_2C_0$ *and* $B_0A_3B_3C_0$ *the coupler points* C *of which trace one and the same coupler curve. Because of this property the three four-bars are said to be cognate.*

The coupler triangles of the three four-bars are similar, but in each triangle another angle is opposite the coupler. Equation (17.72) shows that also the triangle (A_0,B_0,C_0) is similar to the coupler triangle (A_1,B_1,C). For B_2 the sum of the two Eqs.(17.70) yields

$$B_2 = B_1 z \; . \tag{17.73}$$

[4] Samuel Roberts (1827-1913); published 1875

[5] Pavnuty Lvovic Tschebychev (1821-1894); he considers a basic figure with arbitrary coupler triangle, but with identical link lengths $r_1 = r_2$, and he constructs geometrically one other four-bar ([40] p.273 published in 1878)

Hence also the triangle (A_0,B_1,B_2) is similar to the coupler triangle and with the same argument also the triangle (B_0,A_1,B_3).

Imagine that the three four-bars are physically connected at C, and that B_0 and C_0 are free to move. The resulting mechanism is deformable subject to the constraints that (i) links and coupler triangles remain undeformed, and that (ii) parallelograms remain parallelograms. In Fig. 17.16 a position is shown in which the links of four-bar $A_0A_1B_1B_0$ are stretched out in the line $A_0\tilde{A}_1\tilde{B}_1\tilde{B}_0$. The new positions of the remaining points (denoted by the symbol tilde) are determined by the three parallelograms not shaded and by the three similar coupler triangles (shaded). In this position all three four-bars have their links stretched out. The triangle ($A_0\tilde{B}_0\tilde{C}_0$) is similar to the coupler triangles. It is this figure from which all lengths of the other two four-bars are most easily obtained.

Figure 17.15 is particularly simple if the coupler point C in the four-bar $A_0A_1B_1B_0$ is located on the line $\overline{A_1B_1}$ of the coupler. This case is characterized by $\alpha = 0$ or π and z real. From this it follows that in all three four-bars C is located on the coupler line. The positions of C_0, A_2, B_2, A_3 and B_3 are determined by the equations $C_0 = B_0z$, $A_2 = (B_1 - A_1)z$, $B_2 = B_1z$, $B_3 = C + (B_0 - A_1)z$ with real z. Figure 17.17 explains how to proceed geometrically when the four-bar $A_0A_1B_1B_0$ and point C on the coupler are given. As in Fig. 17.15 A_2 and A_3 are constructed by drawing the parallelograms $A_0A_1CA_2$ and $B_0B_1CA_3$. Next, B_2 and B_3 are constructed, the former as point of intersection of the lines $\overline{A_0B_1}$ and $\overline{CA_2}$ and the latter as point of intersection of the lines $\overline{B_0A_1}$ and $\overline{CA_3}$. Finally, C_0 is constructed as in Fig. 17.15 by drawing the parallelogram $B_2CB_3C_0$.

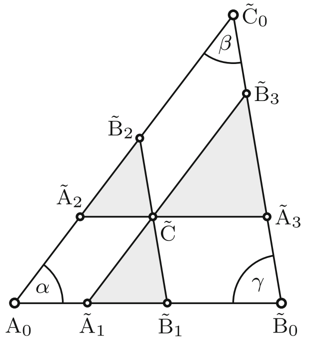

Fig. 17.16 Cognate four-bars of Fig. 17.15 deformed

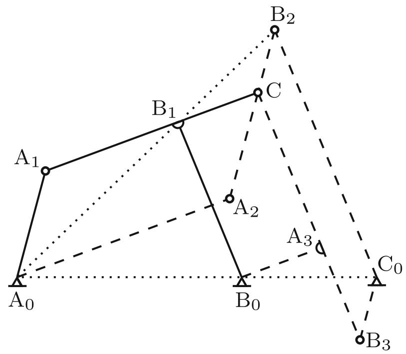

Fig. 17.17 Cognate four-bars with coupler point C on the coupler line

In what follows, the general case shown in Fig. 17.15 is considered again. The parallelity of lines in parallelograms in combination with the rigidity of coupler triangles has the consequences: If one of the links $\overline{A_0A_1}$, $\overline{A_2B_2}$ and

$\overline{C_0B_3}$ is fully rotating, all three of them are fully rotating, and if any one of them is not fully rotating, none of them is fully rotating. The same statements apply to the links $\overline{B_0B_1}$, $\overline{A_3B_3}$ and $\overline{C_0B_2}$. The combination of these arguments leads to the following statements:

1. If four-bar $A_0A_1B_1B_0$ is a double-rocker of second kind, the other two four-bars are double-rockers of second kind as well.
2. If four-bar $A_0A_1B_1B_0$ is a double-crank, the other two four-bars are double-cranks as well.
3. If four-bar $A_0A_1B_1B_0$ is a crank-rocker with crank $\overline{A_0A_1}$, four-bar $A_0A_2B_2C_0$ is double-rocker of first kind, and four-bar $B_0A_3B_3C_0$ is a crank-rocker with crank $\overline{C_0B_3}$.
4. If four-bar $A_0A_1B_1B_0$ is a double-rocker of first kind, the other two four-bars are crank-rockers with cranks $\overline{A_0A_2}$ and $\overline{B_0A_3}$, respectively.

The Roberts-Tschebychev theorem has important engineering applications. If the generation of some particular coupler curve is required and if there is not enough space for the chosen four-bar, the same coupler curve is generated by two other four-bars which are located somewhere else and which are different in size. The same curve can be generated by still other linkages. Equation (17.71), $C_0-B_2=(B_0-B_1)z$, shows that the links $\overline{C_0B_2}$ and $\overline{B_0B_1}$ have identical angular velocities when the four-bars are moving. Identical angular velocities are produced also by means of three gears with centers fixed in the base according to Fig. 17.18a. The two outer gears have arbitrary, but equal diameters, and each of them is rigidly connected with one of the two links. The central gear has arbitrary diameter and arbitrary location. When the central gear is set into motion, C is generating the same coupler curve that is generated by the three four-bars.

The linkage shown in Fig. 17.18b is composed of some of the links in Fig. 17.15. The degree of freedom is two. The parallelogram is free to rotate as rigid body about A_0. It may also deform. Hence it is possible to guide B_1 along an arbitrarily prescribed curve (within a certain workspace). From (17.73), $B_2=B_1z$, it follows that B_2 generates the same curve rotated through the angle α and multiplied by the factor $|z|=\overline{A_1C}/\overline{A_1B_1}$. This linkage is called Sylvester's plagiograph [38], v.3.

If, in particular, B_1 is guided along a straight line f_1 (arbitrary), B_2 is moving along a straight line f_2 which is rotated counter-clockwise against f_1 through α. The links $A_0A_1B_1$ with B_1 guided along f_1 constitute a slider-crank mechanism, and the links $A_0A_2B_2$ with B_2 guided along f_2 constitute another slider-crank mechanism. With both mechanisms the coupler-fixed point C traces one and the same coupler curve. Thus, the existence of two cognate slider-crank mechanisms is proved. The figure explains how to construct one from the other.

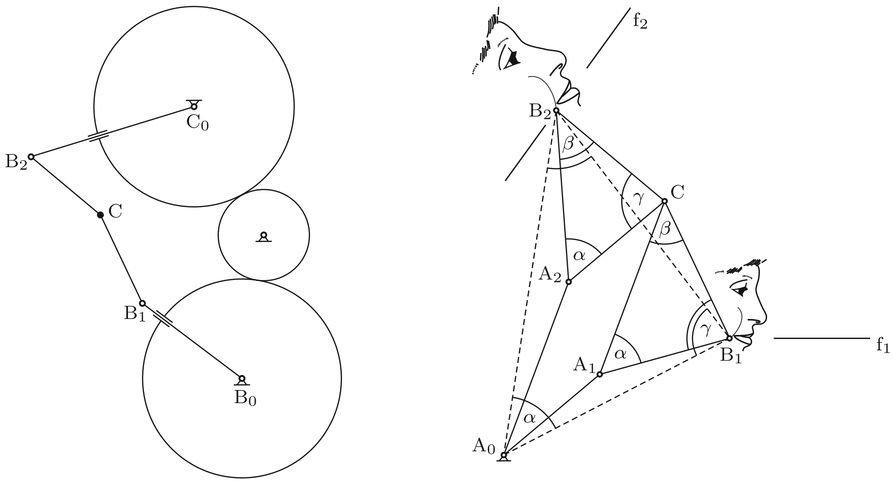

(a) (b)

Fig. 17.18 **Fig. a:** The trajectory of C is identical with the coupler curve generated in Fig. 17.15. **Fig. b:** Sylvester's plagiograph. Cognate slider-crank mechanisms defined by f_1 and f_2

17.8.2 Parameter Equations for Coupler Curves

For the graphical display of coupler curves a parameter representation of the curve is required which determines, in the x, y-system of Fig. 17.19, the coordinates x and y of the coupler point C as functions of the input angle φ. Constant parameters in these functions are ℓ, r_1, r_2, a and the coordinates η and ζ of C in the coupler plane. Using the inclination angle

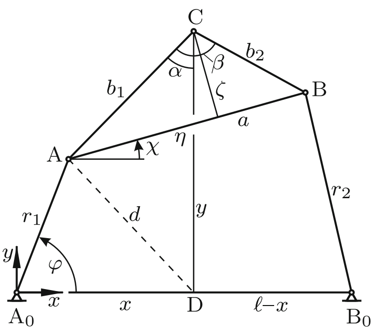

Fig. 17.19 Constant parameters η, ζ, b_1, b_2, β and variable coordinates x, y of the coupler point C

χ of the coupler as auxiliary variable the coordinates of C are

$$x = r_1 \cos\varphi + \eta\cos\chi - \zeta\sin\chi\ , \qquad y = r_1 \sin\varphi + \eta\sin\chi + \zeta\cos\chi\ . \quad (17.74)$$

This is the desired parameter representation of the coupler curve. For $\cos\chi$ and $\sin\chi$ the expressions from (17.23) are substituted:

$$\left.\begin{aligned} \cos\chi_k &= \frac{\bar{A}\bar{C} - (-1)^k \bar{B}\sqrt{\bar{A}^2 + \bar{B}^2 - \bar{C}^2}}{\bar{A}^2 + \bar{B}^2}\ , \\ \sin\chi_k &= \frac{\bar{B}\bar{C} + (-1)^k \bar{A}\sqrt{\bar{A}^2 + \bar{B}^2 - \bar{C}^2}}{\bar{A}^2 + \bar{B}^2}\ , \end{aligned}\right\} (k = 1, 2)\ , \qquad (17.75)$$

$$\bar{A} = -2a(\ell - r_1\cos\varphi)\ , \quad \bar{B} = 2r_1 a\sin\varphi\ , \quad \bar{C} = 2r_1\ell\cos\varphi - (r_1^2 + \ell^2 + a^2 - r_2^2)\ . \quad (17.76)$$

Every input angle φ determines two positions of the four-bar and, hence, two positions of the coupler point C . From Sect. 17.1 it is known that double-rockers of first kind (Fig. 17.4c) and of second kind (Figs. 17.5a,b,c) have the property that the two positions can be reached one from the other by a continuous motion. Hence these four-bars have the property that the coupler curve is unicursal (a single closed curve). In contrast, double-cranks and crank-rockers have the property that the two positions associated with a single input angle cannot be reached one from the other by a continuous motion, but only by disconnection and reassembly (see Figs. 17.4a and b). This has the consequence that coupler curves of such four-bars are bicursal (two closed branches). The transition from unicursal to bicursal coupler curves occurs in foldable four-bars. In this case, the two closed branches of a bicursal curve create a singular point. The three coupler curves in Fig. 17.20 demonstrate the transition from unicursal to bicursal curves. Except for r_1 the sets of parameters $(\ell, r_1, r_2, a, \eta, \zeta)$ are the same for all three curves. The circle is explained following Eq.(17.87).

17.8.3 Implicit Equation for Coupler Curves

Figure 17.19 is considered again. This time, the location of the coupler point C in the coupler plane is specified not by the parameters a, η, ζ, but by the parameters b_1, b_2, β. The transformation equations between these two sets of parameters are

$$\left.\begin{aligned} &b_1 = \sqrt{\eta^2 + \zeta^2}\ , \qquad b_2 = \sqrt{(a - \eta)^2 + \zeta^2}\ , \qquad \cos\beta = \frac{b_1^2 + b_2^2 - a^2}{2b_1 b_2}\ , \\ &a = \sqrt{b_1^2 + b_2^2 - 2b_1 b_2\cos\beta}\ , \quad \eta = \frac{b_1(b_1 - b_2\cos\beta)}{a}\ , \quad \zeta = \frac{b_1 b_2 \sin\beta}{a}\ . \end{aligned}\right\} \quad (17.77)$$

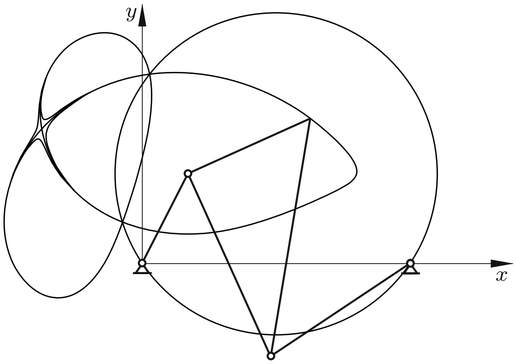

Fig. 17.20 Coupler curves of a double-rocker of second kind with $r_1 = 3.01$ (unicursal), of a foldable four-bar with $r_1 = 3$ and of a crank-rocker with $r_1 = 2.99$ (bicursal). The other parameters $\ell = 8$, $r_2 = 5$, $a = 6$, $\eta = 0$ and $\zeta = 4$ are the same in all three cases. For the circle see (17.87)

For making statements about properties of coupler curves the parameters b_1 , b_2 , β are more suitable. First statements are the following.
In the case $b_1 = 0$ (in the case $b_2 = 0$), coupler curves are circles or arcs of circles with radius r_1 about A_0 (with radius r_2 about B_0). Coupler curves are confined to the area bounded by the concentric circles about A_0 with radii $|r_1 - b_1|$ and $r_1 + b_1$ and by the concentric circles about B_0 with radii $|r_2 - b_2|$ and $r_2 + b_2$. In the case b_1 , $b_2 \gg \ell$, a , r_1 , r_2 , coupler curves are approximately circles or arcs of circles.

The goal of the following analysis is an implicit equation of the coupler curve in the form $f(x, y, \ell, r_1, r_2, b_1, b_2, \beta) = 0$. In developing this equation the auxiliary variables α and d shown in Fig. 17.19 are used temporarily. From the figure it is seen that

$$x = r_1 \cos\varphi + b_1 \sin\alpha \; . \tag{17.78}$$

The cosine law applied to the triangles (A,D,A_0) and (A,D,C) yields two expressions for d^2 . The identity of these expressions is the equation

$$r_1^2 + x^2 - 2xr_1 \cos\varphi = b_1^2 + y^2 - 2b_1 y \cos\alpha \; . \tag{17.79}$$

For $r_1 \cos\varphi$ the expression from (17.78) is substituted. This results in the following equation which is linear with respect to both $\sin\alpha$ and $\cos\alpha$:

$$2b_1(x \sin\alpha + y \cos\alpha) = x^2 + y^2 + b_1^2 - r_1^2 \; . \tag{17.80}$$

The same equations are formulated for the triangles (B,D,C) and (B,D,B_0). They are obtained by replacing in the above equations x , r_1 , b_1 , α by $\ell - x$, r_2 , b_2 , $\beta - \alpha$, respectively. To $\sin(\beta - \alpha)$ and to $\cos(\beta - \alpha)$ addition theorems are applied. The equation equivalent to (17.80) then reads

$$\begin{aligned}&2b_2\Big\{[(x-\ell)\cos\beta+y\sin\beta]\sin\alpha-[(x-\ell)\sin\beta-y\cos\beta]\cos\alpha\Big\}\\&=(x-\ell)^2+y^2+b_2^2-r_2^2\,.\end{aligned}\qquad(17.81)$$

These two equations are solved for $\sin\alpha$ and $\cos\alpha$. Let Δ be the coefficient determinant. It is

$$\Delta=-4b_1b_2[(x^2+y^2)\sin\beta-\ell(x\sin\beta+y\cos\beta)]\,.\qquad(17.82)$$

The solutions are

$$\left.\begin{aligned}\cos\alpha&=\frac{-2}{\Delta}\Big\{b_2(x^2+y^2+b_1^2-r_1^2)[(x-\ell)\cos\beta+y\sin\beta]\\&\qquad-b_1x[(x-\ell)^2+y^2+b_2^2-r_2^2]\Big\}\,,\\\sin\alpha&=\frac{-2}{\Delta}\Big\{b_2(x^2+y^2+b_1^2-r_1^2)[(x-\ell)\sin\beta-y\cos\beta]\\&\qquad+b_1y[(x-\ell)^2+y^2+b_2^2-r_2^2]\Big\}\,.\end{aligned}\right\}\qquad(17.83)$$

Substitution of these expressions into the constraint equation $\cos^2\alpha+\sin^2\alpha=1$ eliminates the auxiliary variable α. The resulting equation is the desired implicit equation of the coupler curve:

$$\begin{aligned}&\Big\{b_2(x^2+y^2+b_1^2-r_1^2)[(x-\ell)\sin\beta-y\cos\beta]\\&\quad+b_1y[(x-\ell)^2+y^2+b_2^2-r_2^2]\Big\}^2\\&+\Big\{b_2(x^2+y^2+b_1^2-r_1^2)[(x-\ell)\cos\beta+y\sin\beta]\\&\quad-b_1x[(x-\ell)^2+y^2+b_2^2-r_2^2]\Big\}^2\\&=4b_1^2b_2^2\Big[(x^2+y^2)\sin\beta-\ell(x\sin\beta+y\cos\beta)\Big]^2\,.\end{aligned}\qquad(17.84)$$

In multiplying out the factor (x^2+y^2) is encountered repeatedly. The equation has the form

$$\begin{aligned}&p_1(x^2+y^2)^3+(x^2+y^2)^2(p_2x+p_3y)+(x^2+y^2)(p_4x^2+p_5xy+p_6y^2\\&+p_7x+p_8y)+p_9x^2+p_{10}xy+p_{11}y^2+p_{12}x+p_{13}y+p_{14}=0\,.\end{aligned}\qquad(17.85)$$

With the abbreviations $p=b_1^2-r_1^2$, $q=\ell^2+b_2^2-r_2^2$, $\lambda=2b_1b_2\cos\beta=b_1^2+b_2^2-a^2$, $a\eta=b_1b_2\sin\beta$ and $a\zeta=b_1(b_1-b_2\cos\beta)$ (see (17.77)) the coefficients are

$$\left.\begin{aligned}
p_1 &= a^2\,, & p_8 &= 2\ell a\zeta(\lambda + r_1^2 + r_2^2 - \ell^2 - a^2)\,,\\
p_2 &= -2\ell a(a+\eta)\,, & p_9 &= Z - 2\ell^2(2a^2\zeta^2 + \lambda p)\,,\\
p_3 &= -2\ell a\zeta\,, & p_{10} &= 4\ell^2 a\zeta(p-\lambda)\,,\\
p_4 &= p_6 + 4\ell^2 a\eta\,, & p_{11} &= Z - \ell^2\lambda^2\,,\\
p_5 &= 4\ell^2 a\zeta\,, & p_{12} &= \ell p(\lambda q - 2b_2^2 p)\,,\\
p_6 &= \ell^2 b_2^2 + p(b_2^2 - b_1^2 - a^2) + 2a(q\eta - 2a\zeta^2)\,, & p_{13} &= -2\ell a\zeta pq\,,\\
p_7 &= \ell\,[\lambda(3p+q) + 8a^2\zeta^2 - 4(b_2^2 p + b_1^2 q)]\,, & p_{14} &= \ell^2 b_2^2 p^2\,,\\
 & & Z &= p(2\ell^2 b_2^2 - \lambda q) + b_2^2 p^2 + b_1^2 q^2\,.
\end{aligned}\right\} \tag{17.86}$$

The highest-order term $p_1(x^2+y^2)^3$ shows that on each of the imaginary lines $y = +\mathrm{i}x$ and $y = -\mathrm{i}x$ the coupler curve has a triple-root at infinity. The curve is a tricircular sextic.

Proposition: An arbitrary circle with center point coordinates x_0, y_0 and with radius r intersects the coupler curve in six (not necessarily real) points. The following proof provides a method for calculating the intersection points. With a parameter γ the circle has the parameter equations $x = x_0 + r\cos\gamma$, $y = y_0 + r\sin\gamma$. This yields $x^2+y^2 = r^2 + x_0^2 + y_0^2 + 2r(x_0\cos\gamma + y_0\sin\gamma)$. These expressions are substituted into (17.85). The result is an equation of third order in $\cos\gamma$ and $\sin\gamma$. The substitution $z = \tan\gamma/2$ leads to a 6th-order polynomial equation for z. End of proof.

The existence of six intersection points of a coupler curve and a circle can be expressed in the following alternative form. Given three circles a , b , c and a triangle (A,B,C), there exist six (not necessarily real) positions of the triangle in which A lies on a , B on b and C on c . This result is important for Sect. 17.10 on planar robots.

The equation $\Delta = 0$ can be written in the form

$$\Big(x - \frac{\ell}{2}\Big)^2 + \Big(y - \frac{\ell}{2}\cot\beta\Big)^2 = \Big(\frac{\ell}{2\sin\beta}\Big)^2\,. \tag{17.87}$$

It is the equation of the circle shown in Fig. 17.21 . The circle passes through A_0 and B_0 . It has the central semi-angle β and, hence, the peripheral angle β . It was shown that β is also the angle at C_0 in the triangle (A_0,B_0,C_0) of Fig. 17.15 . Therefore, also C_0 is located on the circle. From this fact Roberts concluded Theorem 17.2 on the existence of three cognate four-bars generating one and the same coupler curve. The three centers A_0 , B_0 and C_0 are referred to as singular foci, and the circle itself is called *circle of singular foci*. Since Δ equals zero on the circle, $\cos\alpha$ and $\sin\alpha$ are indeterminate if the coupler point is located on the circle. Indeterminate means that at least two different positions of the four-bar generate one and the same point of the coupler curve. In other words: The coupler curve intersects the circle at this point at least twice.

Figure 17.22 proves the inverse statement: If the coupler point C is at one and the same point in two (or more) positions of the four-bar, this multiple point lies on the circle. The coupler triangle is (A_1,B_1,C) in one position

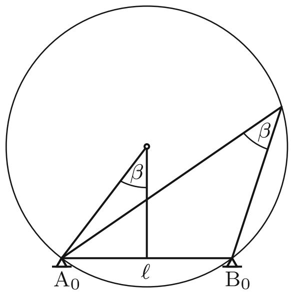

Fig. 17.21 Circle of singular foci

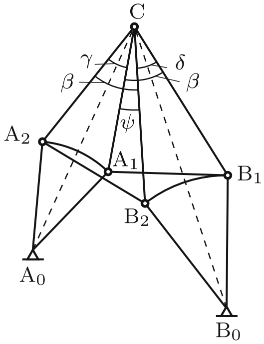

Fig. 17.22 Proof that double points of the coupler curve lie on the circle of singular foci

and (A_2,B_2,C) in the other. It must be shown that $\sphericalangle(A_0,C,B_0)$ equals the angle β in the coupler triangle. The dashed lines $\overline{A_0C}$ and $\overline{B_0C}$ bisect the auxiliary angles γ and δ. With ψ as auxiliary angle $\beta = \gamma + \psi = \delta + \psi$ and, consequently, $\delta = \gamma$. Hence $\sphericalangle(A_0,C,B_0) = \gamma/2 + \psi + \delta/2 = \beta$. End of proof.

There is only a single type of double point of a coupler curve which, in general, is not located on the circle (17.87). This is the singular point on the coupler curve of a foldable four-bar associated with the folded position. It is a point belonging to two branches of the curve and to a single position of the four-bar. Example: The four-bar with parameters $\ell = 8$, $r_1 = 3$, $r_2 = 5$, $a = 6$ is a foldable four-bar. The coupler point $\eta = 0$, $\zeta = 4$ generates the coupler curve shown in Fig. 17.20 which has two ordinary double points on the circle (17.87) and the singular double point related to the folded position.

Conditions for the singular double point to lie on the circle of singular foci are formulated as follows. Let the parameters of the foldable four-bar satisfy the condition $\ell + r_1 = a + r_2$. In the folded position the coupler point C has the coordinates $x = \eta - r_1$, $y = \zeta$. The condition to lie on the circle $\Delta = 0$ is, according to (17.82),

$$[b_1^2 + r_1^2 + r_1\ell - \eta(2r_1 + \ell)]\sin\beta - \zeta\ell\cos\beta = 0 \tag{17.88}$$

and with η and ζ from (17.77)

$$a(b_1^2 + r_1^2 + r_1\ell) - b_1^2(2r_1 + \ell) + 2r_1 b_1 b_2 \cos\beta = 0 \tag{17.89}$$

and with $\cos\beta$ from (17.77)

$$(\ell + r_1 - a)(r_1 a - b_1^2) + r_1 b_2^2 = 0\,. \tag{17.90}$$

With $\ell+r_1-a=r_2$ this is the first equation below. Both equations together constitute the desired conditions.

$$a=\frac{b_1^2}{r_1}-\frac{b_2^2}{r_2}\,,\qquad \ell=a+r_2-r_1\,. \tag{17.91}$$

In terms of dimensionless parameters μ_1, μ_2 the conditions are

$$\left.\begin{aligned} b_1 &= \mu_1 r_1\,, & b_2 &= \mu_2 r_2\,,\\ a &= \mu_1^2 r_1-\mu_2^2 r_2\,, & \ell &= (\mu_1^2-1)r_1-(\mu_2^2-1)r_2\,. \end{aligned}\right\} \tag{17.92}$$

The parameters μ_1, r_1, μ_2, r_2 can be chosen arbitrarily subject to the conditions that (i) $a>0$, (ii) a, b_1, b_2 satisfy the triangle inequalities and (iii) $\ell>0$.

In what follows, four-bars are considered which are not foldable. Like any other circle the circle of singular foci (17.87) intersects a coupler curve at not more than six real points. Hence a coupler curve can have at most three double points. In Fig. 17.23 a coupler curve with three double points is shown. It is generated by a double-rocker with parameters $\ell=10$, $r_1=4$, $a=4$, $r_2=9$, $\eta=2$, $\zeta=4$. Two double points may coincide in a quadruple point. An example is shown in Fig. 17.28.

A double point degenerates into a cusp if the loop associated with the double point contracts into a single point. From this it follows that also cusps lie on the circle (17.87), and that the maximum number of cusps is three. The condition for a cusp to exist is that the coupler point C is located on the moving centrode of the coupler. In the course of rolling of the moving centrode on the fixed centrode the point C generates the cusp when it is the point of contact, i.e., the instantaneous center of rotation of the coupler and, hence, the intersection point of the input and the output link of the four-bar.

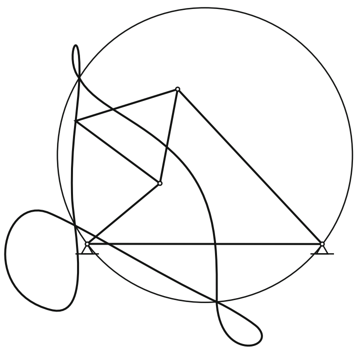

Fig. 17.23 Coupler curve with three double points on the circle with Eq.(17.87). Double-rocker with parameters $\ell=10$, $r_1=4$, $a=4$, $r_2=9$, $\eta=2$, $\zeta=4$

Figure 17.24 demonstrates that this may happen in altogether four different configurations. The common feature is that the segments of lengths (r_1, b_1) and (r_2, b_2) are pairwise collinear. In any such configuration the base $\overline{\mathrm{A_0B_0}}$ is seen from C either under the angle β or under the angle $\pi - \beta$. This proves again that cusps lie on the circle (17.87). In the four-bar $\mathrm{A_0ABB_0}$ drawn with thick lines the cosine law applied to the triangles ($\mathrm{A_0}$,$\mathrm{B_0}$,C) and (A,B,C) yields the equations

$$\left.\begin{aligned} \ell^2 &= (r_1+b_1)^2+(r_2+b_2)^2-2(r_1+b_1)(r_2+b_2)\cos\beta\ ,\\ a^2 &= b_1^2+b_2^2-2b_1b_2\cos\beta\ . \end{aligned}\right\} \qquad (17.93)$$

Elimination of $\cos\beta$ results in a condition for the existence of cusps:

$$b_1b_2[(r_1+b_1)^2+(r_2+b_2)^2-\ell^2]-(r_1+b_1)(r_2+b_2)(b_1^2+b_2^2-a^2)=0\ . \quad (17.94)$$

With reference to Fig. 17.24 (b_1, b_2) can be replaced by $(-b_1, b_2)$, $(b_1, -b_2)$ and $(-b_1, -b_2)$.

Example: To be determined are parameters of coupler curves of foldable four-bars of the kind $\ell+r_1 = a+r_2$ which have not only the singular double point, but also a cusp on the circle of singular foci.
Solution: The parameters must satisfy (17.92) as well as (17.94). Substitution of the expressions (17.92) into (17.94) results in
$(\mu_1+\mu_2-1)[\mu_1(1+\mu_1)r_1-\mu_2(1+\mu_2)r_2]^2 = 0$, i.e.,

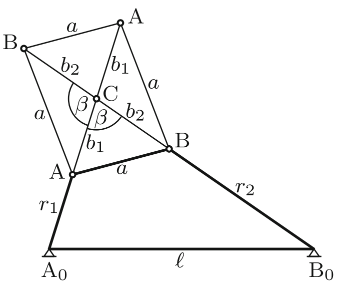

Fig. 17.24 Four different four-bars $\mathrm{A_0ABB_0}$ in positions in which the coupler point C coincides with the instantaneous center of rotation of the coupler thereby passing through a cusp of its coupler curve

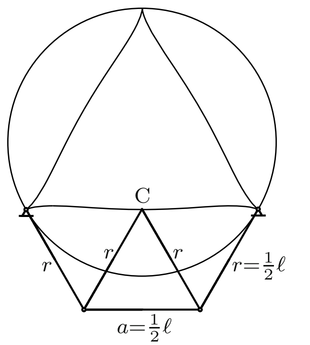

Fig. 17.25 Coupler curve with three cusps on the circle with Eq.(17.87). Symmetrical double-rocker with parameters $r_1 = a = r_2 = b_1 = b_2 = .5\ell$

$$\left.\begin{array}{llll} \text{either} & \mu_2 = 1-\mu_1 & (\,\mu_1\,,\,r_1\,,\,r_2 \text{ arbitrary}) & \text{(a)} \\ \text{or} & r_2 = \dfrac{\mu_1(1+\mu_1)}{\mu_2(1+\mu_2)}r_1 & (\,\mu_1\,,\,\mu_2,\,r_1 \text{ arbitrary}) & \text{(b)}\ . \end{array}\right\} \tag{17.95}$$

As is the case in (17.94) $(\,\mu_1\,,\,\mu_2\,)$ may be replaced by $(\,-\mu_1\,,\,\mu_2\,)$, $(\,\mu_1\,,\,-\mu_2\,)$ and $(\,-\mu_1\,,\,-\mu_2\,)$. Parameters of coupler curves having the desired properties are determined either from (a) or from (b). Condition (b) is a special case. Substitution of this expression for r_2 and of $b_1=\mu_1 r_1$, $b_2=\mu_2 r_2$ into the second Eq.(17.93) shows that $\cos\beta=1$. This means that the generating point of the coupler curve lies on the coupler. End of example.

Figure 17.25 is proof of the existence of coupler curves with three cusps. A coupler curve has three cusps if in one of the three positions both A and B are located on the circle with the diameter $\mathrm{A_0}$–$\mathrm{B_0}$ (Cayley [6] v.9:551–580, Mayer [27]). Let the position drawn in thick lines in Fig. 17.24 be modified so as to satisfy this condition. The angles in the coupler triangle are denoted β, $\sphericalangle(\mathrm{CBA})=\alpha$ and $\sphericalangle(\mathrm{CAB})=\gamma$. Proposition: The triangles $(\mathrm{C,A_0,B_0})$ and (C,A,B) are congruent with $\sphericalangle(\mathrm{CA_0B_0})=\alpha$ and $\sphericalangle(\mathrm{CB_0A_0})=\gamma$. Proof: It suffices to prove the first identity. This is done in three steps.
1. $\sphericalangle(\mathrm{CA_0B})=\pi/2-\beta$ (right-angled triangle).
2. The center 0 of the said circle is the apex of the three isosceles triangles $(\mathrm{A_0,0,A})$, (A,0,B) and $(\mathrm{B,0,B_0})$. The second triangle has the apex angle $\sphericalangle(\mathrm{A0B})=\pi-2\beta$ (twice the angle subtended by A–B). Hence $\sphericalangle(\mathrm{BA0})=\sphericalangle(\mathrm{AB0})=\beta$.
3. The angles $\sphericalangle(\mathrm{CA_0B_0})=\sphericalangle(\mathrm{A_0}A0)$ and $\sphericalangle(\mathrm{CBA})=\alpha$ are both equal to $\pi-\beta-\gamma$. End of proof. The bisected isosceles triangles establish for the internal angles of the triangles the formulas

$$\cos\alpha=\pm\frac{r_1}{\ell}\,,\qquad \cos\beta=\frac{a}{\ell}\,,\qquad \cos\gamma=\pm\frac{r_2}{\ell}\,,\qquad \alpha+\beta+\gamma=\pi\ . \tag{17.96}$$

The signs $\pm$ take into account that, formally, the sign of r_1 and/or r_2 can be reversed. The cosines of the internal angles $\beta_{1,2,3}$ of an arbitrary triangle satisfy the equation[6]

$$\sum_{i=1}^{3}\cos^2\beta_i+2\prod_{i=1}^{3}\cos\beta_i=1\ . \tag{17.97}$$

Hence Eqs.(17.96) are equivalent to

$$\frac{a^2+r_1^2+r_2^2}{\ell^2}\pm 2\,\frac{ar_1r_2}{\ell^3}=1\ . \tag{17.98}$$

This equation shows that ℓ is the largest link length. If two of the three ratios r_1/ℓ, r_2/ℓ, a/ℓ are given, the equation is a quadratic equation for

[6] Proved by substituting $\beta_3=\pi-(\beta_1+\beta_2)$

the third. The ratios determine the angles in the coupler triangle, the side lengths $b_1 = a\sin\alpha/\sin\beta$, $b_2 = a\sin\gamma/\sin\beta$ and the position of the cusp. This cusp is referred to as principal cusp because it is the only one in which both endpoints of the coupler are located on the circle with the diameter $\mathrm{A_0}$–$\mathrm{B_0}$. In the other two positions only one of them is on this circle. More precisely, in the second position the endpoint originally at A has moved to the reflection A′ of A in the line $\overline{\mathrm{A_0B_0}}$, and the cusp is on the line $\overline{\mathrm{A_0A'}}$ at the distance $|r_1 - b_1|$ from $\mathrm{A_0}$. Similarly, in the third position the endpoint originally at B has moved to the reflection B′ of B in the line $\overline{\mathrm{A_0B_0}}$, and the cusp is on the line $\overline{\mathrm{B_0B'}}$ at the distance $|r_2 - b_2|$ from $\mathrm{B_0}$. Simple algebra reveals that the distances of the second and of the third cusp from the principal cusp are $\ell\sin 2\alpha/\sin\beta$ and $\ell\sin 2\gamma/\sin\beta$, respectively. These expressions resemble those for b_1 and b_2. According to the Roberts-Tschebychev Theorem three cusps are generated by three cognate four-bars. Each cusp is the principal cusp for one of these four-bars. In Fig. 17.25 the three cognate four-bars are congruent.

The conditions (17.96) are particularly simple in the case of foldable four-bars. Example: Foldable four-bars of the kind $a + r_2 = \ell + r_1$. With (17.96) this equation is $\cos\beta + \cos\gamma = 1 + \cos\alpha = 1 - \cos(\beta + \gamma)$ or

$$(1 + \cos\beta)\cos\gamma - \sin\beta\sin\gamma = 1 - \cos\beta \; . \tag{17.99}$$

This is an equation for γ in terms of β . It has real roots γ for angles β satisfying the condition $\cos\beta \geq 2 - \sqrt{5}$ ($\beta < 104°$ approximately).

Additional material on coupler curves is found in Mayer [27] and Müller [28, 30, 31].

17.8.4 Symmetrical Coupler Curves

Coupler curves which are symmetrical with respect to the base line $\overline{\mathrm{A_0B_0}}$ have an Eq.(17.84) in which y appears in terms of even orders only. For this it is necessary that $\sin\beta = 0$. This means that the generating coupler point C lies on the coupler line $\overline{\mathrm{AB}}$ (not necessarily between the points A and B). The coupler curve in Fig. 17.2 is an example. According to the Roberts-Tschebychev theorem every such coupler curve is generated by two more four-bars. Also in these four-bars the coupler point lies on the coupler line.

In Eq.(17.84) for symmetrical coupler curves with $\sin\beta = 0$ the parameters are $b_1 = \eta$ and $b_2 = \eta - a$ where η is the parameter used in Fig. 17.19 . Of particular interest are intersection points of the coupler curve with the axis of symmetry. With $y = 0$ the following equation is obtained for these points which is of third order in x and in η :

$$(\eta - a)(x - \ell)(x^2 + \eta^2 - r_1^2) - \eta x[(x - \ell)^2 + (\eta - a)^2 - r_2^2] = 0 \,. \quad (17.100)$$

For given parameters the equation has either one or three real roots x. For this reason one does not expect coupler curves which do not intersect the x-axis. Such coupler curves do exist, however. Example: If $\eta = 2a$ and $r_2 = a$, the equation has the roots $x_1 = \ell$ and $x_{2,3} = \ell \pm \sqrt{4a^2 + \ell^2 - r_1^2}$. For the parameter values $\ell = 1$, $a = 1.3$ and $r_1 = 0.4$ the three roots are real. Yet, the coupler curve does not intersect the x-axis. In Fig. 17.38 the branch of this curve above the x-axis is shown. The three real roots are marked B_0, P_1 and P_2. They represent singular points of the coupler curve. In order to understand this phenomenon (17.80) and (17.81) must be formulated for the special case $b_1 = \eta$, $b_2 = \eta - a$, $\beta = 0$, $y = 0$:

$$x^2 + \eta^2 - 2x\eta \sin\alpha = r_1^2 \,, \qquad (x - \ell)^2 + (\eta - a)^2 - 2(x - \ell)(\eta - a)\sin\alpha = r_2^2 \,. \quad (17.101)$$

Each equation expresses the cosine law for one of the triangles of Fig. 17.13. The elimination of $\sin\alpha$ is possible without imposing the constraint equation $\cos^2\alpha + \sin^2\alpha = 1$. Simple linear combination of the equations results in (17.100). Only those real solutions of this equation are admissible solutions for which Eqs.(17.101) yield $|\sin\alpha| \le 1$.

Symmetrical coupler curves of a different nature are generated if the four-bar and the coupler triangle satisfy the symmetry conditions $r_1 = r_2 = r$ and $b_1 = b_2 = b$, respectively. Fig. 17.26 shows the system in its symmetrical trapezoidal position. The coupler curve of point C is symmetrical with respect to the midnormal of the base $\overline{A_0B_0}$. The figure shows also one of the cognate four-bars which, according to the Roberts-Tschebychev theorem, generate the same coupler curve. The third four-bar is the reflection of the second in the midnormal of the base $\overline{A_0B_0}$. The parameters of the second four-bar are denoted r'_1, a', r'_2, b'_1, b'_2. They satisfy the condition $r'_2 = b'_2 = a'$. Hence also this is a sufficient condition for the coupler curve to be symmetric. The symmetry axis passes through C_0, and its inclination angle against the base line $\overline{C_0A_0}$ is $\beta/2$. The angle at C is $\beta' = \pi/2 - \beta/2$.

In Fig. 17.27 this kind of four-bar $A_0A_1B_1B_0$ with coupler point C is shown again, but this time with the usual notation, i.e., $r_2 = b_2 = a$ instead of $r'_2 = b'_2 = a'$ and β instead of β'. The length of the input link is r. The symmetry axis of the coupler curve passes through B_0 under the angle $\pi/2 - \beta$ against the base line. The symmetry axis is made the y-axis of an x, y-system with origin B_0. At B_1 the transmission angle 2α is shown. It is convenient to use α as independent variable for the x, y-coordinates of C. From isosceles triangles with the apex B_1 the auxiliary quantities ϱ and d are obtained:

$$\varrho = 2a\cos(\alpha - \beta) \,, \qquad d = 2a\sin\alpha \,. \quad (17.102)$$

The angle δ appears also in the triangle (A_0, B_0, A_1). The cosine law $r^2 = d^2 + \ell^2 - 2d\ell\cos\delta$ yields

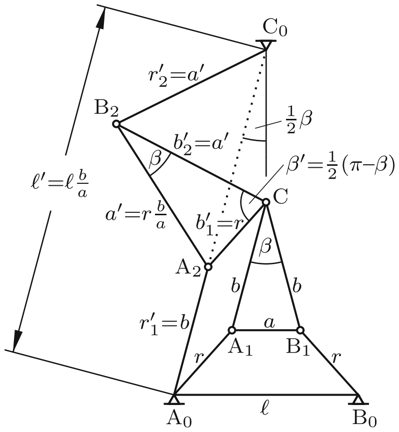

Fig. 17.26 Cognate four-bars generating a symmetrical coupler curve

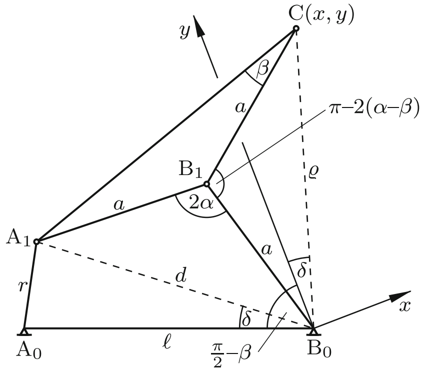

Fig. 17.27 Four-bar generating a coupler curve with symmetry axis y

$$\cos\delta = \frac{4a^2\sin^2\alpha + \ell^2 - r^2}{4a\ell\sin\alpha} \tag{17.103}$$

With these expressions the coordinates of C are

$$\begin{aligned} y &= \varrho\cos\delta = \frac{4a^2\sin^2\alpha + \ell^2 - r^2}{2\ell\sin\alpha}\,\cos(\alpha-\beta) \\ &= \frac{1}{2\ell}\Big[4a^2(\cos\beta\sin\alpha\cos\alpha + \sin\beta\sin^2\alpha) \\ &\qquad + (\ell^2 - r^2)(\sin\beta + \cos\beta\cot\alpha)\Big]\,, \end{aligned} \tag{17.104}$$

$$\begin{aligned} x &= \pm\varrho\sin\delta = \pm\sqrt{\varrho^2 - y^2} \\ &= \pm\sqrt{4a^2\cos^2(\alpha-\beta) - y^2}\,. \end{aligned} \tag{17.105}$$

These equations find an application in Sect. 17.12.3.

From the figure it is seen that intersection points of the coupler curve with the symmetry axis are characterized by $\delta = 0$. In such positions A_1 lies on the base line. Then either $d = \ell - r$ or $d = \ell + r$ and $y = \varrho$. Equations (17.102) yield the associated angles α and the stationary values y:

$$\sin\alpha = \frac{\ell \mp r}{2a}\,, \qquad y = 2a\cos(\alpha-\beta)\,. \tag{17.106}$$

The position $d = \ell - r$ is always possible, the position $d = \ell + r$ only if the four-bar is a crank-rocker. It is left to the reader to show that the positions $d = \ell - r$ and $d = \ell + r$ of a crank-rocker yield identical values of y if the parameters satisfy the condition $r^2 + \ell^2\cot^2\beta = 4a^2\cos^2\beta$. In this case, the coupler curve has a quadruple point on the circle of singular foci. In Fig. 17.28 these conditions are satisfied.

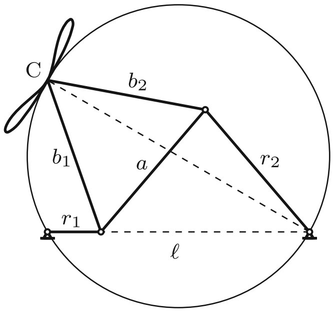

Fig. 17.28 Symmetrical coupler curve with quadruple point on the circle of singular foci. Crank-rocker with parameters $\ell = 2\sqrt{6}$, $r_1 = 1$, $r_2 = a = b_1 = b_2 = 3$

17.9 Slider-Crank. Inverted Slider-Crank

The slider-crank mechanism shown in Fig. 17.29a is derived from the four-bar in Fig. 17.19 by moving the point B_0 in y-direction to $-\infty$. This has the effect that the endpoint B of the coupler of length a is guided along the straight line $y = h =$ const. In the inverted slider-crank mechanism of Fig. 17.29b the coupler of length a has become the fixed link, while the fixed link with the parameter h has become the moving coupler. The parameter h can be positive or zero or negative. Arbitrarily, it is considered as positive in both figures. In both figures the crank angle φ is the input variable, and the inclination angle χ of the coupler and the position s of the slider are output variables. Every value of φ is associated with two positions of the mechanism. In Fig. 17.29a the two values of χ and s are determined by the equations

$$\sin\chi_{1,2} = \frac{h - r\sin\varphi}{a}\ , \qquad s_{1,2} = r\cos\varphi \pm \sqrt{a^2 - (h - r\sin\varphi)^2}\ . \quad (17.107)$$

In Fig. 17.29b the output variables are obtained from two equations expressing the fact that the slider has the coordinates $x = a$ and $y = 0$:

$$r\cos\varphi + h\cos\chi + s\sin\chi = a\ , \qquad r\sin\varphi + h\sin\chi - s\cos\chi = 0\ . \quad (17.108)$$

Decoupling produces the equations

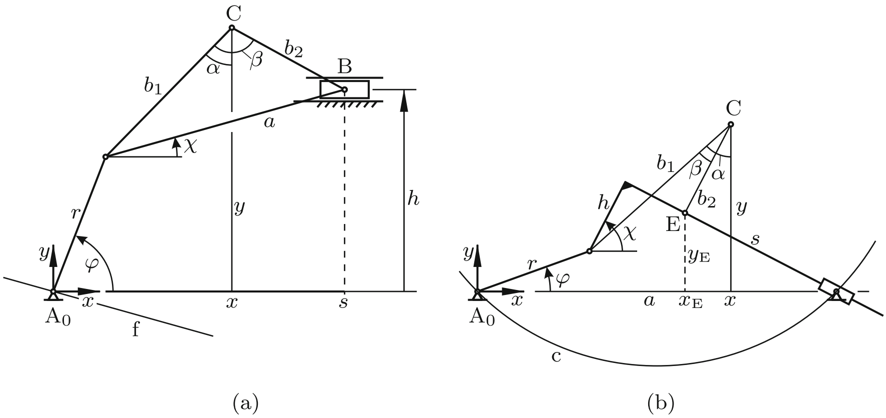

Fig. 17.29 Slider-crank **(a)** and inverted slider-crank **(b)**

$$\left.\begin{array}{l}(r\cos\varphi - a)\cos\chi + r\sin\varphi\sin\chi = -h\ ,\\ s = r\sin\varphi\cos\chi - (r\cos\varphi - a)\sin\chi\ .\end{array}\right\}\qquad(17.109)$$

The first equation has two solutions $\cos\chi_{1,2}$ and $\sin\chi_{1,2}$. The associated solutions $s_{1,2}$ are obtained from the second equation. In both figures the equivalent to Grashof's Theorem 17.1 is

Theorem 17.3. *The link with the shorter of the two lengths a and r is fully rotating relative to all other links if*

$$h^2 \le (a-r)^2\ .\qquad(17.110)$$

Coupler curves: In both figures the coupler-fixed point C is specified by constant parameters b_1, b_2 and β. In Fig. 17.29a the notation is the same as in Fig. 17.19, whereas in Fig. 17.29b b_2 and β are defined differently. Implicit equations for coupler curves in the form $f(x,y,r,b_1,b_2,\beta)=0$ are obtained from two linear equations for the sine and cosine of the auxiliary variable angle α. For both figures (17.78) and (17.79) are valid. Hence also the resulting Eq.(17.80) is valid:

$$2b_1(x\sin\alpha + y\cos\alpha) = x^2 + y^2 + b_1^2 - r^2\ .\qquad(17.111)$$

In Fig. 17.29a the second linear equation for $\cos\alpha$ and $\sin\alpha$ is

$$y = h + b_2\cos(\beta-\alpha)\ .\qquad(17.112)$$

In Fig. 17.29b the coordinates of point E satisfy the three equations

$$x_E = x - b_2\sin(\alpha-\beta)\ ,\quad y_E = y - b_2\cos(\alpha-\beta)\ ,\quad x_E = a - y_E\cot(\alpha-\beta)\ .\qquad(17.113)$$

Elimination of $x_{\rm E}$ and $y_{\rm E}$ produces the desired second linear equation:

$$(x-a)\sin(\alpha-\beta)+y\cos(\alpha-\beta)=b_2\ . \tag{17.114}$$

To this equation and to (17.112) addition theorems are applied. Following this, the two sets of equations, one for Fig. 17.29a and one for Fig. 17.29b, are solved for $\cos\alpha$ and $\sin\alpha$. As in Eqs.(17.83) for the four-bar these solutions have the forms $\cos\alpha=U/\Delta$ and $\sin\alpha=V/\Delta$ with the pertinent coefficient determinants U, V and Δ. The desired implicit equations of the coupler curves are the equations $\cos^2\alpha+\sin^2\alpha=1$, i.e., $U^2+V^2=\Delta^2$. The equation $\Delta=0$ determines the locus of double points and cusps of coupler curves. Omitting elementary intermediate steps only the final equations are documented.

Figure 17.29a: The equation of the coupler curve is the quartic

$$\begin{aligned}&\Big[b_2(x^2+y^2+b_1^2-r^2)\sin\beta-2b_1x(y-h)\Big]^2\\ &+\Big[b_2(x^2+y^2+b_1^2-r^2)\cos\beta-2b_1y(y-h)\Big]^2\\ &=4b_1^2b_2^2(x\cos\beta-y\sin\beta)^2\ .\end{aligned} \tag{17.115}$$

The equation $\Delta=0$ defines the straight line (line f in Fig. 17.29a)

$$y=x\cot\beta\ . \tag{17.116}$$

Since a straight line intersects a quartic in at most four real points, the maximum number of double points and of cusps is two. In the context of Fig. 17.18b the existence of two cognate slider-crank mechanisms producing one and the same coupler curve has been proved.

Figure 17.29b: The equation of the coupler curve is the tricircular sextic

$$\begin{aligned}&\Big\{(x^2+y^2+b_1^2-r^2)[y\sin\beta+(x-a)\cos\beta]-2b_1b_2x\Big\}^2\\ &+\Big\{(x^2+y^2+b_1^2-r^2)[y\cos\beta-(x-a)\sin\beta]-2b_1b_2y\Big\}^2\\ &=4b_1^2\Big\{x[y\cos\beta-(x-a)\sin\beta]-y[y\sin\beta+(x-a)\cos\beta]\Big\}^2\ .\end{aligned} \tag{17.117}$$

The equation $\Delta=0$ defines the circle of singular foci (circle c in Fig. 17.29b)

$$\Big(x-\frac{a}{2}\Big)^2+\Big(y-\frac{a}{2}\cot\beta\Big)^2=\Big(\frac{a}{2\sin\beta}\Big)^2\ . \tag{17.118}$$

This equation is formally identical with Eq.(17.87) for the four-bar. Both a and ℓ denote the length of the fixed link. The definitions of β are different, however. The maximum number of double points and of cusps of coupler curves on the circle is three. It can be shown that the third singular focus coincides with the singular focus A_0. This has the consequence that there are no cognate inverted slider-crank mechanisms.

17.10 Planar Parallel Robot

The triangular platform (A,B,C) of the planar parallel robot in Fig. 17.30 is positioned by means of three telescopic arms with controllable lengths r_i ($i = 1, 2, 3$) which are pivoted at A_0, B_0, C_0. The platform serves as carrier of tools or of work pieces[7]. The characterization as *parallel* points to the fact that the platform is positioned by arms in a parallel arrangement in contrast to a *serial* robot where it is positioned by a single arm with a series of links and joints (see Sect. 5.7). Parallel robots are able to manipulate heavier loads than serial robots, and they position them with higher accuracy and with greater stiffness.

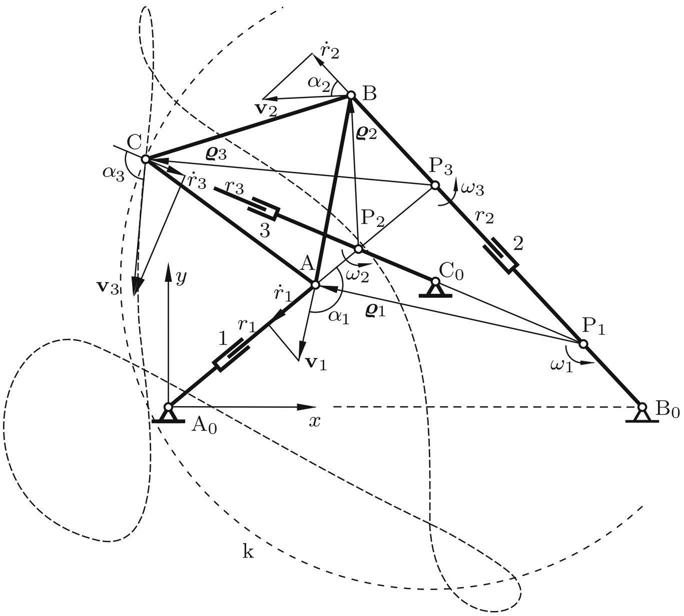

Fig. 17.30 Planar parallel robot. Four-bar A_0ABB_0 with coupler curve generated by C. The rate of change $\dot{r}_3$ of the leg length r_3 causes the platform to rotate with angular velocity $\omega_3 = \dot{r}_3/(\varrho_3 \cos\alpha_3)$ about P_3

---

[7] Other types of three-legged planar robots see in Hayes/Husty [21]

The planar parallel robot poses the following kinematics problem. Altogether nine parameters are given. These are three quantities specifying the triangle (A,B,C), the arm lengths r_i $(i = 1, 2, 3)$ and, in the x, y-system shown, the x-coordinate of B_0 and the x, y-coordinates of C_0. To be determined are all possible positions of the triangle (A,B,C).

Solution: Imagine that joint C connecting the platform with arm 3 is eliminated. Point C is located on the coupler curve generated by C fixed to the four-bar A_0ABB_0 and also on the circle k of radius r_3 about C_0. The four-bar and the coupler curve in Fig. 17.30 are copied from Fig. 17.23. The circle k intersects the coupler curve at six points. This is the maximum possible number of points. How to calculate these points was explained following (17.85). Each point determines a possible position of the robot. This concludes the position analysis.

Next, the velocity state is analyzed. Imagine that the telescopic joint in arm 3 is a passive joint so that this arm adapts itself freely to motions of the four-bar A_0ABB_0 with fixed lengths r_1 and r_2. The platform (A,B,C) has relative to the base the instantaneous center P_3 at the intersection of arms 1 and 2. Let $\boldsymbol{\omega}_3$ be the angular velocity of the coupler ($\omega_3 > 0$ counterclockwise). The velocity of C is $\mathbf{v}_3 = \boldsymbol{\omega}_3 \times \boldsymbol{\varrho}_3$. It is tangent to the coupler curve. As is shown α_3 denotes the angle between $\mathbf{r}_3$ and $\mathbf{v}_3$ in the case $\omega_3 > 0$. Arm 3 changes its length with the velocity $\dot{r}_3 = \omega_3 \varrho_3 \cos\alpha_3$. Conversely, if $\dot{r}_3$ is prescribed, $\omega_3 = \dot{r}_3/(\varrho_3 \cos\alpha_3)$. This angular velocity and the instantaneous center P_3 determine the velocities of A, B and C. The formula for ω_3 shows that $\dot{r}_3 \neq 0$ is possible only if in the position under investigation the coupler curve and the circle k are not in tangential contact. The quantities ϱ_3 and $\cos\alpha_3$ are calculated from the triangle (C_0, P_3, C).

Similar statements are valid when in the position under investigation arm 1 only or arm 2 only experiences a rate of change of length $\dot{r}_1$ or $\dot{r}_2$, respectively. In Fig. 17.30 also the instantaneous centers P_1, P_2 together with the associated quantities $\boldsymbol{\varrho}_1$, α_1 and $\boldsymbol{\varrho}_2$, α_2 are shown. When the three rates of change $\dot{r}_1$, $\dot{r}_2$, $\dot{r}_3$ occur simultaneously, the superposition principle yields the resultant angular velocity

$$\omega = \sum_{i=1}^{3} \frac{\dot{r}_i}{\varrho_i \cos\alpha_i} \,. \tag{17.119}$$

The velocity of each of the points A, B, C is the sum of three velocities two of which are collinear. The instantaneous center of the platform is the intersection point of the normals of the velocities of A, B and C.

17.11 Four-Bars with Prescribed Transmission Characteristics

The transmission characteristic is the relation between input angle φ and output angle ψ. In what follows, the implicit form (17.9) is used:

$$-\ell r_1 \cos\varphi + \ell r_2 \cos\psi = r_1 r_2 \cos(\varphi - \psi) + \frac{1}{2}[a^2 - (r_1^2 + \ell^2 + r_2^2)] \; . \quad (17.120)$$

It depends upon the three parameters r_1/ℓ, r_2/ℓ and a/ℓ where ℓ is a given unit length. In some engineering applications it is required that a four-bar produces prescribed pairs of input and output angles (φ_k, ψ_k) $(k = 1, 2, \ldots)$. In other applications it is required that some prescribed function $\psi = f(\varphi)$ be optimally approximated over a certain interval $0 \le \varphi \le \varphi_{\max}$. These and related problems have been treated extensively in the literature (see, for example, Lichtenheldt/Luck [26], Hain [18, 19], Soni [36]). In what follows, a few problems are discussed in detail.

17.11.1 Prescribed Pairs of Input-Output Angles

First, the case is treated that three pairs of angles (φ_k, ψ_k) $(k = 1, 2, 3)$ are prescribed. Equation (17.120) yields the three equations

$$-\ell r_1 \cos\varphi_k + \ell r_2 \cos\psi_k = r_1 r_2 \cos(\varphi_k - \psi_k) + \frac{1}{2}[a^2 - (r_1^2 + \ell^2 + r_2^2)] \quad (17.121)$$

$(k = 1, 2, 3)$. The differences first minus second and second minus third equation have the general forms

$$A_1 \ell r_1 + B_1 \ell r_2 = C_1 r_1 r_2 \; , \qquad A_2 \ell r_1 + B_2 \ell r_2 = C_2 r_1 r_2 \qquad (17.122)$$

with given constants A_i, B_i, C_i $(i = 1, 2)$. Division by $r_1 r_2$ results in two linear equations for ℓ/r_1 and ℓ/r_2 with uniquely determined real solutions. These solutions are substituted into one of the Eqs.(17.121). This equation then determines a^2/ℓ^2. The solution thus obtained is useful only if, first, $r_1 > 0$, $r_2 > 0$, $a^2/\ell^2 > 0$ and, second, the four-bar with these link lengths is capable of producing the prescribed pairs of angles in the desired order and without disconnection and reassembly.

In most engineering applications it is not required that the four-bar produces prescribed pairs of angles (φ_k, ψ_k) $(k = 1, 2, \ldots)$. Instead, pairs of angular differences $(\varphi_k - \varphi_0, \psi_k - \psi_0)$ $(k = 1, 2, \ldots)$ are prescribed where the pair (φ_0, ψ_0) is an *unspecified initial position* of the four-bar. The angles φ_0 and ψ_0 are free parameters so that the total number of free parameters is five. In this formulation of the problem (17.120) must be satisfied for the pair (φ_0, ψ_0) and for up to four pairs $(\varphi_0+\varphi_k, \psi_0+\psi_k)$ $(k = 1, 2, 3, 4)$. The previous discussion has shown that results may be useless for various reasons (negative or imaginary link lengths, wrong order etc.). Therefore, only three pairs $(\varphi_0 + \varphi_k, \psi_0 + \psi_k)$ $(k = 1, 2, 3)$ are prescribed. This has the consequence, that the solutions for ψ_0, r_1, r_2 and a are functions of φ_0. This initial angle φ_0 is a free parameter which is chosen later so as to arrive at a useful solution. The altogether four equations are

$$-\ell r_1 \cos\varphi_0 + \ell r_2 \cos\psi_0 = r_1 r_2 \cos(\varphi_0 - \psi_0) + \frac{1}{2}[a^2 - (r_1^2 + \ell^2 + r_2^2)] \,, \quad (17.123)$$

$$\begin{aligned} -\ell r_1 \cos(\varphi_0 + \varphi_k) + \ell r_2 \cos(\psi_0 + \psi_k) &= r_1 r_2 \cos(\varphi_0 + \varphi_k - \psi_k - \psi_0) \\ &+ \frac{1}{2}[a^2 - (r_1^2 + \ell^2 + r_2^2)] \qquad (k = 1, 2, 3) \,. \quad (17.124) \end{aligned}$$

The first equation is subtracted from each of the remaining three equations. The differences are then divided by $r_1 r_2$. This results in the equations

$$\begin{aligned} &\frac{\ell}{r_2}[\cos(\varphi_0 + \varphi_k) - \cos\varphi_0] - \frac{\ell}{r_1}[\cos(\psi_0 + \psi_k) - \cos\psi_0] \\ &= \cos(\varphi_0 - \psi_0) - \cos(\varphi_0 + \varphi_k - \psi_k - \psi_0) \qquad (k = 1, 2, 3) \,. \quad (17.125) \end{aligned}$$

These are three linear inhomogeneous equations for ℓ/r_1 and ℓ/r_2. For a solution to exist it is necessary that the (3×3)-coefficient determinant including the right-hand side terms be zero. This condition results in an equation in which φ_0 and ψ_0 are the only unknowns. In order to be able to express ψ_0 as function of φ_0 Eqs.(17.125) are rewritten with the help of addition theorems in such a way that $\cos\psi_0$ and $\sin\psi_0$ are isolated. The equations thus rewritten are

$$\left.\begin{aligned} &a_k \frac{\ell}{r_2} + (b_k \cos\psi_0 + c_k \sin\psi_0)\frac{\ell}{r_1} = d_k \cos\psi_0 + f_k \sin\psi_0 \,, \\ &a_k = \cos(\varphi_0 + \varphi_k) - \cos\varphi_0 \,, \quad d_k = \cos\varphi_0 - \cos(\varphi_0 + \varphi_k - \psi_k) \,, \\ &b_k = 1 - \cos\psi_k \,, \qquad\qquad\quad\;\; f_k = \sin\varphi_0 - \sin(\varphi_0 + \varphi_k - \psi_k) \,, \\ &c_k = \sin\psi_k \end{aligned}\right\} \quad (17.126)$$

$(k = 1, 2, 3)$. The condition is

$$\begin{vmatrix} a_1 & b_1 \cos\psi_0 + c_1 \sin\psi_0 & d_1 \cos\psi_0 + f_1 \sin\psi_0 \\ a_2 & b_2 \cos\psi_0 + c_2 \sin\psi_0 & d_2 \cos\psi_0 + f_2 \sin\psi_0 \\ a_3 & b_3 \cos\psi_0 + c_3 \sin\psi_0 & d_3 \cos\psi_0 + f_3 \sin\psi_0 \end{vmatrix} = 0 \qquad (17.127)$$

or explicitly

$$A\cos^2\psi_0 + B\sin^2\psi_0 + 2C\cos\psi_0\sin\psi_0 = 0\ , \tag{17.128}$$

$$\left.\begin{aligned} A &= a_1(b_2d_3-b_3d_2)+a_2(b_3d_1-b_1d_3)+a_3(b_1d_2-b_2d_1)\ ,\\ B &= a_1(c_2f_3-c_3f_2)+a_2(c_3f_1-c_1f_3)+a_3(c_1f_2-c_2f_1)\ ,\\ C &= \tfrac{1}{2}[a_1(b_2f_3-b_3f_2)+a_2(b_3f_1-b_1f_3)+a_3(b_1f_2-b_2f_1)\\ &\quad + a_1(c_2d_3-c_3d_2)+a_2(c_3d_1-c_1d_3)+a_3(c_1d_2-c_2d_1)]\ . \end{aligned}\right\} \tag{17.129}$$

In the special case $A = B \neq 0$, the solutions are $\psi_0 = -\frac{1}{2}\sin^{-1}(A/C)$ and $\psi_0 = \pi - \frac{1}{2}\sin^{-1}(A/C)$. In the special case $A \neq 0$, $B = 0$, the solutions are $\psi_0 = \pm\pi/2$ and $\psi_0 = -\frac{1}{2}\tan^{-1}A/(2C)$ and $\psi_0 = \pi - \frac{1}{2}\tan^{-1}A/(2C)$. In all other cases division by $\cos^2\psi_0$ results in the quadratic equation $B\tan^2\psi_0 + 2C\tan\psi_0 + A = 0$. Each solution $\tan\psi_0$ determines two angles ψ_0 which differ by $180°$. With each real solution ψ_0 two out of the three Eqs.(17.126) determine r_1/ℓ and r_2/ℓ. With these solutions r_1/ℓ and r_2/ℓ (17.123) determines a^2/ℓ^2. At this point the desired formulation of the unknowns ψ_0, r_1, r_2 and a as functions of the free parameter φ_0 is accomplished. The variation of φ_0 in search of a useful solution must be done numerically.

17.11.2 Prescribed Transmission Ratios

In this section four-bars are determined which produce two prescribed pairs of angles (φ_k, ψ_k) $(k = 1, 2)$ and, in the second position (φ_2, ψ_2), a prescribed value i_2 of the transmission ratio $i = \dot\varphi/\dot\psi$. The first two conditions yield the equations (see (17.121))

$$-\ell r_1\cos\varphi_k + \ell r_2\cos\psi_k = r_1r_2\cos(\varphi_k - \psi_k) + \frac{1}{2}[a^2 - (r_1^2 + \ell^2 + r_2^2)] \tag{17.130}$$

$(k = 1, 2)$. As before, the difference of these two equations produces the first Eq.(17.122). For the transmission ratio (17.31) is used. This yields an equation of the same type:

$$-\ell r_1\sin\varphi_2 + \frac{\ell r_2}{i_2}\sin\psi_2 = r_1r_2\Big(1 - \frac{1}{i_2}\Big)\sin(\varphi_2 - \psi_2)\ . \tag{17.131}$$

This is the second Eq.(17.122). The further steps of solution are as before.

The method of solution for five parameters (see (17.123), (17.124)) remains the same if one or two of the Eqs.(17.124) are replaced by the requirement that the transmission ratio is prescribed for one or two of the remaining pairs of angles.

17.11.3 Jeantaud's Steering Mechanism

In an automobile the steering mechanism causes the axes of the front wheels to turn about points A_0 and B_0 fixed in the car body. In Fig. 17.31 the axes are shown in a vertical projection during a left turn. With an ideal steering mechanism the turning angles α and β are coordinated such that the two front axes and the rear axis of the car have, independent of the radius R of the curve, a common intersection point. The lengths ℓ and h are constant parameters. From triangles the equations are obtained: $h = (R - \ell/2) \tan\alpha$, $h = (R + \ell/2) \tan\beta$. Elimination of the variable R results in

$$\cot\beta - \cot\alpha = \frac{\ell}{h}\,. \tag{17.132}$$

This equation defines the function $\beta(\alpha)$. It is an odd function. The curve denoted k in Fig. 17.32 is the graph of this function for the specific parameter value $\ell/h = 0.5$ in the interval of interest up to the maximum steering angles $(\alpha_{\max}, \beta_{\max})$. If, for example, $\alpha_{\max} = 40°$, (17.132) yields $\beta_{\max} \approx 30.6°$.

Jeantaud invented the steering mechanism shown in Fig. 17.33 . It is a symmetrical four-bar approximating (17.132). The input link and the output link of equal length r are rotating about A_0 and B_0 , respectively. They are rigidly connected with the front axes. The figure shows the mechanism in the symmetrical trapezoidal position (front axes not turned) and in a

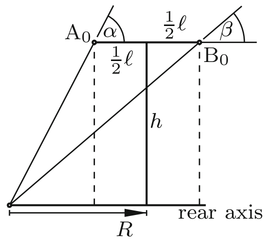

Fig. 17.31 Ideal turning angles α and β of the front axes of a car during a turn

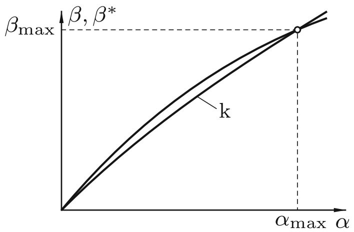

Fig. 17.32 Graph of the function $\beta = f(\alpha)$ for $\ell/h = 0.5$ (curve k) and approximation by a Jeantaud mechanism with nonoptimal parameters (ϱ, γ)

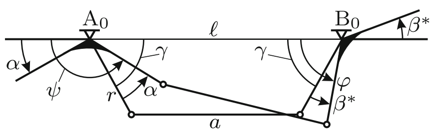

Fig. 17.33 Jeantaud mechanism

position effecting a left turn. The link lengths are ℓ, r and a. Suitable dimensionless parameters are $\varrho = r/\ell$ and the angle γ. The figure shows that $a = \ell - 2r\cos\gamma$. Hence

$$2r^2+\ell^2-a^2 = 2r^2+4r\ell(1-\varrho\cos\gamma)\cos\gamma = 2r\ell(2\cos\gamma-\varrho\cos 2\gamma)\ . \quad (17.133)$$

The turning angle of the left front axis is α. The angle of the right axis is called not β, but β^* because it is an approximation of β. The figure shows angles ψ and φ. When this figure is rotated 180°, it has the form and the notation of Fig. 17.7. Equation (17.9) relating φ and ψ is

$$2r\ell(\cos\psi - \cos\varphi) - 2r^2\cos(\varphi-\psi) + 2r^2 + \ell^2 - a^2 = 0\ . \quad (17.134)$$

For $2r^2+\ell^2-a^2$ the expression in (17.133) is substituted. Figure 17.33 shows that $\varphi = \gamma + \beta^*$ and $\psi = \pi + \alpha - \gamma$. Also these substitutions are made. When the resulting equation is divided by $2r\ell$, it has the form

$$\cos(\gamma+\beta^*) + \cos(\gamma-\alpha) - \varrho\cos(2\gamma+\beta^*-\alpha) = 2\cos\gamma - \varrho\cos 2\gamma\ . \quad (17.135)$$

After applying the addition theorem for the cosine function this takes the form

$$A\cos\beta^* + B\sin\beta^* = C\ , \quad (17.136)$$

$$\left.\begin{array}{l} A = \cos\gamma - \varrho\cos(2\gamma-\alpha)\ , \quad C = 2\cos\gamma - \varrho\cos 2\gamma - \cos(\gamma-\alpha)\ , \\ B = -\sin\gamma + \varrho\sin(2\gamma-\alpha)\ . \end{array}\right\} \quad (17.137)$$

The equation has two solutions β^*. Their sines are

$$\sin\beta^* = \frac{BC \pm A\sqrt{A^2+B^2-C^2}}{A^2+B^2}\ . \quad (17.138)$$

The pertinent solution is the one which has the same sign that α has. This solution defines a two-parametric manifold of functions $\beta^*(\alpha,\varrho,\gamma)$ with parameters ϱ and γ. Every parameter combination (ϱ,γ) determines a curve $\beta^*(\alpha)$ in the diagram of Fig. 17.32. It is reasonable to require that the curve passes through the point $\alpha = \alpha_{\max}$, $\beta^* = \beta_{\max}$. This means that (17.135) is satisfied with $\alpha = \alpha_{\max}$ and $\beta^* = \beta_{\max}$. This equation determines for every value of γ the associated value of ϱ. Thus, a one-parametric manifold of curves with parameter γ is left. In Fig. 17.32 a single nonoptimal curve is shown. The optimal value of γ is determined from the criterion that the maximum of the deviation $|\beta^*(\alpha)-\beta(\alpha)|$ in the interval $0 \le \alpha \le \alpha_{\max}$ be minimal. It turns out that this criterion yields two solutions $\gamma_1 > 0$ and $\gamma_2 < 0$. Example: With $\ell/h = 0.5$, $\alpha_{\max} = 40^\circ$ and $\beta_{\max} \approx 30.6^\circ$ the solutions are $\gamma_1 \approx 67^\circ$, $\varrho_1 \approx 0.25$ and $\gamma_2 \approx -121^\circ$, $\varrho_2 \approx 0.25$. The four-bar with γ_2 is located in front of the front axis. The four-bar with γ_1 is the one shown in Fig. 17.33. It is located behind the front axis (Brossard [4]).

17.12 Coupler Curves with Prescribed Properties

A problem frequently encountered in engineering is the design of a four-bar for the generation of a coupler curve having certain prescribed properties. If the four-bar has to be a crank-rocker, a suitable design may be found in the book by Hrones/Nelson [22]. It is a compilation of 7300 coupler curves. In each diagram a single crank-rocker is shown together with coupler curves for a variety of coupler-fixed points. A different ordering principle of coupler curves is found in Volmer [41]. Each diagram is a compilation of four-bars (not only crank-rockers) and of coupler curves having the same singular foci and the same double points on the circle of singular foci (17.87). In what follows, some mathematical problems and methods of solution are discussed which are encountered in the generation of coupler curves with prescribed properties.

17.12.1 Coupler Curves Passing Through Prescribed Points

The parameter representation of the coupler curve in the form of Eqs.(17.74) – (17.76) contains the six constant parameters ℓ, r_1, r_2, a, η, ζ and as seventh parameter the variable φ. These equations describe the coupler curve in the special x, y-system of Fig. 17.19. Three additional constant parameters determine the location of this x, y-system in an x', y'-reference system.

In a typical problem statement it is required that a coupler curve passes through prescribed points in the x', y'-system. Also the order in which these points are passed is prescribed. Let m be the number of prescribed points. The $2m$ prescribed coordinates result in $2m$ conditional equations. These equations contain $9 + m$ free parameters, namely, the nine constant parameters listed above and for every prescribed point the associated crank angle. From the equality $2m = 9 + m$ it follows that up to nine points can be prescribed. To be sure, not for every set of nine prescribed points real solutions exist and if they are real, the nine points are, in general, not passed in the prescribed order. It may happen that the calculated coupler curve is bicursal with some of the nine points on each branch.

The number m of points that can be prescribed is smaller than nine if the additional requirement exists that the angle $\varphi_k - \varphi_1$ of rotation of the input crank associated with the passage from point P_1 to point P_k is prescribed for $k = 2, \ldots, m$. The only free angle is φ_1. This means that altogether ten free parameters exist while the number of equations to be satisfied is $2m$ as before. From the equality $2m = 10$ it follows that at most five points can be prescribed. Methods for solving this problem see in Freudenstein [15] and Dijksman [8].

17.12.2 Straight-Line Approximations

Coupler curves with approximately straight-line segments have important engineering applications (see Fig. 17.2). The earliest straight-line approximation was invented by Watt[8] for the purpose of guiding the piston in his steam engine. His four-bar is a symmetrical double-rocker of second kind with link lengths ℓ, r_1, a, r_2 satisfying the conditions $r_1 = r_2 = r$ and $\ell = 2\sqrt{r^2 + (a/2)^2}$. The ratio a/r is a free parameter. In Fig. 17.34a the four-bar with link lengths $r = 35$, $a = 24$ and $\ell = 74$ is shown in four positions. The figure-eight-shaped coupler curve generated by the midpoint C of the coupler is symmetric to both the base line $\overline{\mathrm{A_0B_0}}$ and the midnormal of this base line. The maximum distance from the base line (in position 4 of point C) is $\sqrt{a(\ell - a)/2}$.

Watt was unaware of cognate four-bars since the Roberts-Tchebychev theorem had not yet been discovered. So was Evans who invented the so-called *grashopper linkage* shown in Fig. 17.34b . It is a cognate of Watt's mechanism. Positions 1, 2, 3, 4 of the coupler point C are the same as in Fig. 17.34a . Evans' linkage has the advantage of being half the size of Watt's mechanism for one and the same coupler curve.

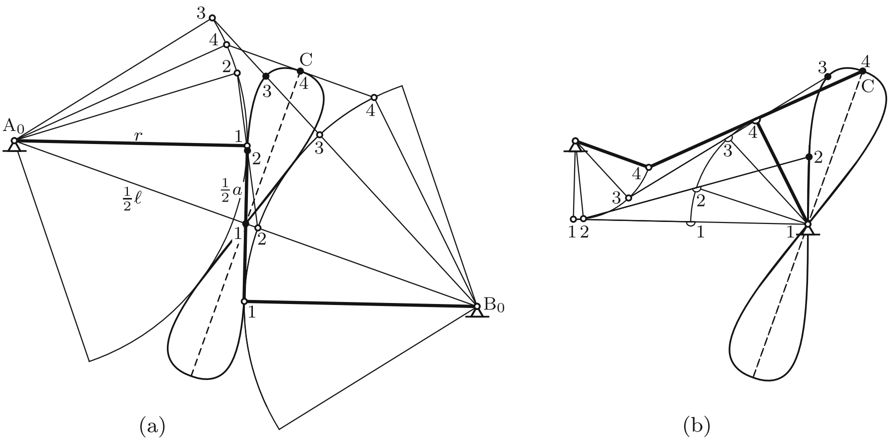

Fig. 17.34 Watt's straight-line approximation by a double-rocker with $r = 35$, $a = 24$, $\ell = 74$ **(a)** and Evans' grashopper linkage **(b)** , a cognate of Watt's mechanism

[8] James Watt (1736-1819) nowadays primarily known for the invention of steam engines wrote: "Though I am not over anxious after fame, yet I am more proud of the parallel motion than of any other mechanical invention I have ever made"

Roberts[9] is the inventor of another straight-line approximation (see Fig. 17.35). The coupler curve is symmetric with respect to the midnormal of the base. In the symmetry position shown the coupler point C is on the base line (coupler length $a = \ell/2$, coupler triangle with $b_1 = b_2 = r$). The three congruent triangles are determined by the single parameter $\varrho = r/\ell$. In the figure the case $\varrho = .6$ is shown. The coupler curve has a cusp and double points at A_0 and B_0.

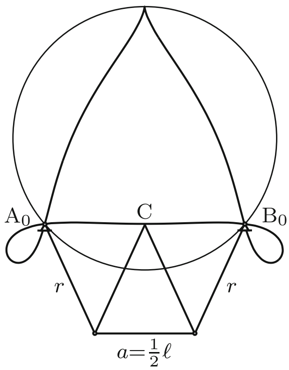

Fig. 17.35 Roberts' straight-line approximation by the double-rocker with $r/\ell = .6$

Remark on the influence of the parameter ϱ: With $\varrho = 1/2$ the coupler curve has three cusps. This curve is shown in Fig. 17.25. With every $\varrho > 1/2$ the coupler curve has a single cusp and double points at A_0 and B_0. The midpoint between A_0 and B_0 is a minimum. The maximum deviation $\Delta_{\max}$ from the straight line between A_0 and B_0 occurs at two symmetrically located maxima. With increasing ϱ this $\Delta_{\max}$ tends monotonically toward zero[10]. In the same process the straight-line approximation becomes increasingly better in an increasingly longer interval extending beyond the points A_0 and B_0. With $\varrho = 3/4$ the four-bar is foldable. With $\varrho > 3/4$ the coupler is fully rotating. From an engineering point of view large values of ϱ are impractical.

Watt's, Evans' and Roberts' straight-line approximations were found by engineering intuition. A more systematic approach was explained in Sect. 15.3.6. The coupler curve of the point which, in a position under investigation, is Ball's point of the coupler is a good straight-line approximation, because it has at this point zero curvature and zero rate of change of curvature. A textbook entirely devoted to straight-line approximations (by means of four-bars and of other linkages) is Kraus [25]. Straight-line approximations by means of inverted slider-crank mechanisms see also in Wunderlich [46]. By

[9] Richard Roberts (1789-1864), not to be confused with Samuel Roberts (1827-1913) of the Roberts/Tschebychev theorem

[10] $\Delta_{\max}/\ell \approx .0154$ for $\varrho = .5$, $\Delta_{\max}/\ell \approx .0068$ for $\varrho = .6$, $\Delta_{\max}/\ell \approx .0029$ for $\varrho = .75$

far the best straight-line approximations by coupler curves of four-bars were obtained by Tschebychev [39, 40] who used this problem for demonstrating the power of a new and widely applicable approximation theory invented by him. His method is the subject of the next section.

17.12.3 Tschebychev's Straight-Line Approximations

The general problem solved by Tschebychev is the following. In a given interval $x_a \le x \le x_b$ a given function $F(x)$ is to be approximated by another function of the form

$$P_n(x, p_0, \ldots, p_n) = p_0 f_0(x) + \ldots + p_n f_n(x) \tag{17.139}$$

with free parameters $p_0, \ldots, p_n$ and with *given* linearly independent functions $f_0(x), \ldots, f_n(x)$. Tschebychev proved

Theorem 17.4. *If the function $P_n(x, p_0, \ldots, p_n)$ has at most n real roots in the interval $x_a \le x \le x_b$, uniquely determined parameters $p_0, \ldots, p_n$ exist such that the maximum of the absolute value of the approximation error $\Delta_n(x, p_0, \ldots, p_n) = P_n(x, p_0, \ldots, p_n) - F(x)$ in the interval $x_a \le x \le x_b$ is minimal:*

$$|\Delta_n(x, p_0, \ldots, p_n)|_{\max} = Min! \qquad (x_a \le x \le x_b)\,. \tag{17.140}$$

Moreover, if D is this maximum, the optimal function $\Delta_n(x, p_0, \ldots, p_n)$ attains in the interval $x_a \le x \le x_b$ alternatingly not less than $(n+2)$ times extremal values D and $-D$.

For a proof of the theorem see Tschebychev [39] (p.111 and 273), Watson [45] and Powell [34]. Figure 17.36 shows schematically the graph of the optimal function Δ_n in the case $n = 2$. At the boundaries x_a and x_b and at unspecified points x in the interval $x_a \le x \le x_b$ the maximum D and the minimum $-D$ are attained not less than four times. Points x of extremal values in the interval are double roots of one of the two equations

$$\Delta_n(x, p_0, \ldots, p_n) \pm D = 0\,. \tag{17.141}$$

Extrema at the boundaries x_a and x_b of the interval are either simple roots or double roots of (17.141). Double roots satisfy also the equation

$$\Delta_n'(x, p_0, \ldots, p_n) = 0\,. \tag{17.142}$$

The $n+2$ Eqs.(17.141) and the n Eqs.(17.142) for double roots x in the interior of the interval represent altogether $2n+2$ equations. This equals the

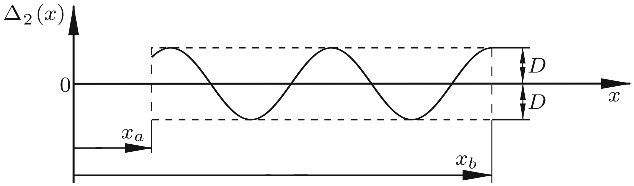

Fig. 17.36 Optimal function $\Delta_2(x, p_0, p_1, p_2)$ with extrema D and $-D$ inside and on the boundaries of the interval $x_a \le x \le x_b$

number of unknowns. Unknown are D, $p_0, \ldots, p_n$ and the n double roots x in the interior of the interval. Thus, it is possible to express all unknowns in terms of x_a and x_b. The equations are linear with respect to D, p_0, ..., p_n and they are nonlinear with respect to the double roots x in the interior of the interval.

Remarks: 1. The set of Eqs.(17.141) does not change if D is replaced by $-D$. For this reason D is redefined as either maximum or minimum of the function.

2. If in (17.140) the function Δ_n is replaced by $\lambda\Delta_n$ with an arbitrary constant λ, the solutions for p_0, ..., p_n, x_1, ..., x_{n+2} remain unaltered, but D is replaced by λD.

Now back to straight-line approximations. In [40] p.51 Tschebychev investigated the family of coupler curves which are symmetric with respect to the midnormal of the base $\overline{\mathrm{A_0B_0}}$ and among these coupler curves those which approximate a straight line parallel to the base. Roberts' coupler curve belongs to this family. Watt's does not. For the family of symmetric coupler curves the parameter Eqs.(17.104), (17.105) based on Fig. 17.27 are used[11]:

$$\left.\begin{aligned} y(\alpha) &= \frac{1}{2\ell}\Big[4a^2(\cos\beta\sin\alpha\cos\alpha + \sin\beta\sin^2\alpha) \\ &\qquad + (\ell^2 - r^2)(\sin\beta + \cos\beta\cot\alpha)\Big]\,, \\ x(\alpha) &= \pm\sqrt{4a^2\cos^2(\alpha-\beta) - y^2}\,. \end{aligned}\right\} \tag{17.143}$$

The symmetry-axis is the y-axis. The constant parameters of the four-bar are ℓ, r, a, β, and the free parameter is the angle α. Intersection points of the coupler curve with the y-axis are associated with one of the angles (see (17.106))

$$\sin\alpha = \frac{\ell \mp r}{2a}\,. \tag{17.144}$$

[11] The four-bar analyzed in [40] p.51 is the one with symmetries $r_1 = r_2$ and $b_1 = b_2$. Only later Tschebychev [40] p.273 discovered what is now known as Roberts/Tschebychev theorem. The formulation presented here follows the exposition in Artobolevski/Levitski/Cherkudinov [2] without, however, making the substitution $z = \sin^2\alpha$

Tschebychev determined parameters ℓ, r, a, β such that the coupler curve is the optimal approximation to a straight line $y = y_0 =$ const. The difference $y(\alpha) - y_0$ or rather a constant multiple of it is the function $\Delta_n = P_n - F$. With $n = 2$ it is written in the form

$$\Delta_2 = \frac{2\ell}{(\ell^2 - r^2)\cos\beta}\,[y(\alpha) - y_0] = p_0 f_0(\alpha) + p_1 f_1(\alpha) + p_2 f_2(\alpha) - F(\alpha) \tag{17.145}$$

with the following functions and coefficients

$$f_0(\alpha) = 1\,, \quad f_1(\alpha) = \sin\alpha\cos\alpha\,, \quad f_2(\alpha) = \sin^2\alpha\,, \quad F(\alpha) = -\cot\alpha\,, \tag{17.146}$$

$$p_0 = \tan\beta - \frac{2y_0\ell}{(\ell^2 - r^2)\cos\beta}\,, \qquad p_1 = \frac{4a^2}{\ell^2 - r^2}\,, \qquad p_2 = \frac{4a^2\tan\beta}{\ell^2 - r^2}\,. \tag{17.147}$$

In this formulation the problem appears as approximation of the function $F(\alpha) = -\cot\alpha$ by $P_2 = p_0 f_0 + p_1 f_1 + p_2 f_2$. In the interval $0 \le \alpha \le \pi$ the function P_2 has at most two real roots. In the segment of the coupler curve which is of interest the inequality $0 < \alpha < \pi/2$ holds. Thus, the conditions for the applicability of Tschebychev's theorem are satisfied. Equations (17.141) read:

$$p_0 + p_1 \sin\alpha\cos\alpha + p_2\sin^2\alpha + \cot\alpha \pm D = 0\,. \tag{17.148}$$

According to the theorem each equation has (at least) one simple root and one double root in the interval $0 < \alpha < \pi/2$. This is, indeed, the case. The equations can be written in the forms

$$\left.\begin{aligned} \sin(\alpha - \alpha_1)\sin^2(\alpha - \alpha_3) = 0\,, \\ \sin(\alpha - \alpha_4)\sin^2(\alpha - \alpha_2) = 0 \end{aligned}\right\} \tag{17.149}$$

with constants $0 < \alpha_1, \ldots, \alpha_4 < \pi/2$. For the first equation this is shown as follows. With an addition theorem and after division through $\sin\alpha\sin\alpha_1\sin^2\alpha_3$ the equation has the form

$$(\cot\alpha_1 - \cot\alpha)[1 + (\cot^2\alpha_3 - 1)\sin^2\alpha - 2\cot\alpha_3\sin\alpha\cos\alpha] = 0\,. \tag{17.150}$$

Multiplying out further leads to

$$\begin{aligned} \cot\alpha_1 &+ 2\cot\alpha_3 + (1 - 2\cot\alpha_1\cot\alpha_3 - \cot^2\alpha_3)\sin\alpha\cos\alpha \\ &+ [(\cot^2\alpha_3 - 1)\cot\alpha_1 - 2\cot\alpha_3]\sin^2\alpha - \cot\alpha = 0\,. \end{aligned} \tag{17.151}$$

This is indeed Eq.(17.148). In the case $+D$, comparison of coefficients yields

$$p_0 = -\cot\alpha_1 - 2\cot\alpha_3 - D\,, \tag{17.152}$$

$$\left.\begin{aligned} p_1 &= \cot^2\alpha_3 + 2\cot\alpha_1\cot\alpha_3 - 1 = \frac{2\sin(\alpha_1+2\alpha_3)}{(1-\cos 2\alpha_3)\sin\alpha_1}\ , \\ p_2 &= 2\cot\alpha_3 + (1-\cot^2\alpha_3)\cot\alpha_1 = -\frac{2\cos(\alpha_1+2\alpha_3)}{(1-\cos 2\alpha_3)\sin\alpha_1}\ . \end{aligned}\right\} \tag{17.153}$$

In the same way the second Eq.(17.149) and Eq.(17.148) with $-D$ yield

$$p_0 = -\cot\alpha_4 - 2\cot\alpha_2 + D\ , \tag{17.154}$$

$$p_1 = \frac{2\sin(\alpha_4+2\alpha_2)}{(1-\cos 2\alpha_2)\sin\alpha_4}\ , \qquad p_2 = -\frac{2\cos(\alpha_4+2\alpha_2)}{(1-\cos 2\alpha_2)\sin\alpha_4}\ . \tag{17.155}$$

The results obtained so far are summarized as follows. Each of the equations $\Delta_2 = \pm D$ has in the interval $0 < \alpha < \pi/2$ a simple root (α_1 or α_4) and a double root (α_2 or α_3). Suppose that $\alpha_1 < \alpha_4$. The graph of the optimal function Δ_2 is as shown in Fig. 17.36 with α instead of x . The roots α_1 and α_4 are the boundaries of the approximation interval.

The six Eqs.(17.152) – (17.155) suffice for determining the unknowns D , p_0 , p_1 , p_2 , α_2 and α_3 as functions of α_1 and α_4 . The two Eqs.(17.142), which are valid for $x = \alpha_2$ and for $x = \alpha_3$, are not needed because Eqs.(17.148) are available in the explicit form (17.149). Solutions for the unknowns are obtained as follows. Equations (17.152) and (17.154) yield

$$p_0 = -\frac{1}{2}(\cot\alpha_4 + \cot\alpha_1) - (\cot\alpha_3 + \cot\alpha_2)\ , \tag{17.156}$$

$$D = \frac{1}{2}(\cot\alpha_1 - \cot\alpha_4) + (\cot\alpha_3 - \cot\alpha_2)\ . \tag{17.157}$$

With (17.153) and (17.155)

$$\frac{p_1}{p_2} = -\tan(\alpha_1 + 2\alpha_3) = -\tan(\alpha_4 + 2\alpha_2)\ . \tag{17.158}$$

From this it follows that either

$$\alpha_1 + 2\alpha_3 = \alpha_4 + 2\alpha_2 \tag{17.159}$$

or $\alpha_1 + 2\alpha_3 = \alpha_4 + 2\alpha_2 + \pi$. From these two equations and from (17.153) and (17.155) it follows that either

$$(1-\cos 2\alpha_3)\sin\alpha_1 = (1-\cos 2\alpha_2)\sin\alpha_4 \tag{17.160}$$

or $(1-\cos 2\alpha_3)\sin\alpha_1 = -(1-\cos 2\alpha_2)\sin\alpha_4$. Because of the restriction $0 < \alpha_1, \alpha_4 < \pi/2$ only (17.159) together with (17.160) is useful. Equation (17.159) yields

$$\alpha_3 = \alpha_2 + \frac{1}{2}(\alpha_4 - \alpha_1)\ . \tag{17.161}$$

With the corresponding expression $\cos 2\alpha_3 = \cos 2\alpha_2 \cos(\alpha_4 - \alpha_1) - \sin 2\alpha_2 \sin(\alpha_4 - \alpha_1)$ Eq.(17.160) becomes an equation for α_2 :

$$\begin{aligned}&[\sin\alpha_4 - \sin\alpha_1 \cos(\alpha_4 - \alpha_1)] \cos 2\alpha_2 \\ &+ \sin\alpha_1 \sin(\alpha_4 - \alpha_1) \sin 2\alpha_2 = \sin\alpha_4 - \sin\alpha_1 \;. \end{aligned} \tag{17.162}$$

Of its two solutions for α_2 only one is located between α_1 and α_4. Only this solution is useful. The associated angle α_3 is calculated from (17.161). Following this, Eqs.(17.155) – (17.157) determine p_0, p_1, p_2 and D as functions of α_1 and α_4.

The three Eqs.(17.147) relate the seven quantities α_1, α_4, ℓ, y_0, r, a and β. These relations are expressed as follows. Equating the two expressions for p_0 in (17.147) and (17.156) yields for y_0 the expression shown below. Similarly, equating the two expressions for p_1 in (17.147) and (17.153) yields for a^2 the expression shown below. Finally, equating the expressions for p_2/p_1 in (17.147) and (17.158) yields for $\tan\beta$ the two expressions shown below.

$$y_0 = \frac{\ell^2 - r^2}{2\ell} \cos\beta \left[\tan\beta + \frac{1}{2}(\cot\alpha_4 + \cot\alpha_1) + (\cot\alpha_3 + \cot\alpha_2) \right] , \tag{17.163}$$

$$a^2 = (\ell^2 - r^2) \frac{\sin(\alpha_1 + 2\alpha_3)}{2(1 - \cos 2\alpha_3)\sin\alpha_1} , \tag{17.164}$$

$$\tan\beta = -\cot(\alpha_1 + 2\alpha_3) = -\cot(\alpha_4 + 2\alpha_2) \;. \tag{17.165}$$

Four out of the seven quantities α_1, α_4, ℓ, y_0, r, a and β can (within certain limits) be prescribed arbitrarily. The base length ℓ is prescribed as unit length. The interval boundaries α_1 and α_4 are associated with certain points (x_1, y_1) and (x_4, y_4), respectively, of the coupler curve which are determined by (17.143). It is the segment of the coupler curve between these points which is approximated to the straight line $y = y_0$. Now, it is decided that one of these points, say (x_1, y_1), is located on the symmetry axis. Because of the symmetry this has the consequence that the coupler curve is approximated in the segment of double length between the points $(-x_4, y_4)$ and (x_4, y_4). According to (17.144) the condition $x_1 = 0$ has one of the forms $\sin\alpha_1 = (\ell \mp r)/(2a)$. By an investigation which is omitted here it can be shown that a better approximation of the straight line $y = y_0$ is achieved when the plus sign is chosen:

$$\sin\alpha_1 = \frac{\ell + r}{2a} \;. \tag{17.166}$$

The angle α_1 is real only if the four-bar to be determined is a crank-rocker. Whether the results satisfy this condition remains to be seen.

The third quantity we prescribe is $\beta = 0$. This means that the coupler point lies on the coupler line. Having made these decisions on ℓ, α_1 and β

a one-parametric manifold of four-bars is left. As parameter the ratio

$$\varrho = \frac{r}{\ell} \tag{17.167}$$

is chosen. It should be noted that Roberts' four-bar is a double-rocker with an angle $\beta \neq 0$. Thus, the straight-line approximations to be determined are of a different nature[12].

The next task is to express the quantities y_0 and a in (17.163) and (17.164) in terms of ℓ and ϱ. In addition, two new quantities are defined which are measures of quality of the approximation. These are the relative length $L/\ell = 2x_4/\ell = 2x(\alpha_4)/\ell$ of the approximately straight segment and the relative width $B/L = 2(y-y_0)_{\max}/L$ of the error in this segment. These quantities are expressed in terms of ϱ. This is done first for B/ℓ. Equations (17.145) and (17.157) yield the preliminary expression

$$\begin{aligned}\frac{B}{\ell} &= \frac{2(y-y_0)_{\max}}{\ell} = \frac{\ell^2 - r^2}{\ell^2}\,D \\ &= (1-\varrho^2)\Big[\frac{1}{2}(\cot\alpha_1 - \cot\alpha_4) + (\cot\alpha_3 - \cot\alpha_2)\Big] .\end{aligned} \tag{17.168}$$

With $\beta = 0$ Eqs.(17.165) take the simple forms

$$2\alpha_3 = \frac{\pi}{2} - \alpha_1 , \qquad 2\alpha_2 = \frac{\pi}{2} - \alpha_4 . \tag{17.169}$$

With these expressions (17.160) becomes
$(1-\sin\alpha_1)\sin\alpha_1 = (1-\sin\alpha_4)\sin\alpha_4$.
This has the trivial solution $\alpha_4 = \alpha_1$ and the significant solution

$$\sin\alpha_4 = 1 - \sin\alpha_1 . \tag{17.170}$$

The first Eq.(17.169) yields $\sin(\alpha_1 + 2\alpha_3) = 1$ and $\cos 2\alpha_3 = \sin\alpha_1$ or with (17.166) $\cos 2\alpha_3 = (\ell + r)/(2a)$. Substitution of these expressions into (17.164) leads to

$$a = \frac{\ell}{2}(3-\varrho) . \tag{17.171}$$

The parameter ϱ is free subject to the condition that the four-bar is a crank-rocker. For this to be the case, $r = \varrho\ell$ must be the shortest link. In addition, Grashof's inequality (17.4), $\ell_{\min} + \ell_{\max} \leq \ell' + \ell''$, must be satisfied. Both conditions are satisfied if and only if $0 < \varrho \leq 1$.

The expression obtained for a is substituted back into (17.166). With this equation and with (17.169) and (17.170) the formulas are obtained:

[12] Tschebychev [40] (p.273, p.285, p.301 and p.495) investigated also the case $\beta \neq 0$. Also for this case he gave explicit formulas for a one-parametric family of four-bars. In [40] p.495 the approximation of a circle is investigated

$$\left.\begin{aligned}
\sin\alpha_1 &= \frac{1+\varrho}{3-\varrho}\,, \qquad \cos\alpha_1 = \frac{2\sqrt{2(1-\varrho)}}{3-\varrho}\,, \qquad \cot\alpha_3 = \frac{1+\sin\alpha_1}{\cos\alpha_1}\,,\\
\sin\alpha_4 &= 2\frac{1-\varrho}{3-\varrho}\,, \qquad \cos\alpha_4 = \frac{\sqrt{(5-3\varrho)(1+\varrho)}}{3-\varrho}\,, \qquad \cot\alpha_2 = \frac{1+\sin\alpha_4}{\cos\alpha_4}\,.
\end{aligned}\right\} \tag{17.172}$$

With these expressions (17.163) and (17.168) yield for the location y_0 of the straight line and for the measure of quality B/ℓ the formulas

$$\frac{y_0}{\ell} = \sqrt{2(1-\varrho)} + \frac{1}{8}(5-3\varrho)\sqrt{(5-3\varrho)(1+\varrho)}\,, \tag{17.173}$$

$$\frac{B}{\ell} = 2\sqrt{2(1-\varrho)} - \frac{1}{4}(5-3\varrho)\sqrt{(5-3\varrho)(1+\varrho)}\,. \tag{17.174}$$

For the ratio L/ℓ Eqs.(17.143) yield

$$\begin{aligned}
y_4 &= \frac{1}{2\ell}\cot\alpha_4[(3\ell-r)^2\sin^2\alpha_4 + \ell^2 - r^2]\\
&= \frac{\ell}{4}(5-3\varrho)\sqrt{(5-3\varrho)(1+\varrho)}\,,
\end{aligned}\tag{17.175}$$

$$\begin{aligned}
\frac{L}{\ell} &= \frac{2x_4}{\ell} = \frac{2}{\ell}\sqrt{(3\ell-r)^2\cos^2\alpha_4 - y_4^2}\\
&= \frac{1}{2}\sqrt{3(5-3\varrho)(1+\varrho)(3-\varrho)(3\varrho-1)}\,.
\end{aligned}\tag{17.176}$$

From L/ℓ and B/ℓ the second measure of quality B/L is calculated.

$L > 0$ requires that $\varrho > 1/3$. The diagram in Fig. 17.37 shows as functions of ϱ the ratios L/ℓ and $|B/L|$ characterizing the quality of the straight-line approximation. The former should be large and the latter very small. These goals are achieved with values of ϱ close to $1/3$.

Example: With $\varrho = r/\ell = .4$ (17.171), (17.173), (17.176) and (17.174), determine the coupler length $a = 1.3\ell$, the length $y_0 \approx 2.19\ell$ and the measures of quality $L/\ell \approx 1.44$ and $|B/L| \approx .00020$. This is an excellent straight-line approximation. The entire coupler curve is shown in Fig. 17.38. The four-bar is drawn in solid lines. Dashed lines show the cognate four-bar generating the same coupler curve. For the significance of the points B_0, P_1 and P_2 see the comment following (17.100). For comparison: The straight-line approximations by Watt / Evans (Fig. 17.34a,b) and by Roberts (Fig. 17.35) are not nearly as good. The measures of quality for Roberts' approximation are $L/\ell \approx 1$ and $|B/L| \approx .0068$. From Fig. 17.37 it is seen that with increasing ϱ the measure of quality L/ℓ improves while the essential measure of quality $|B/L|$ deteriorates. For $\varrho = r/\ell = .5$, for example, the measures are $L/\ell \approx 2.22$ and $|B/L| \approx .0022$. This is still a very good straight-line approximation. End of example.

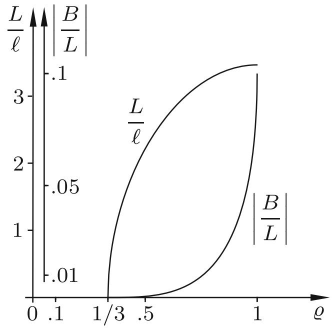

Fig. 17.37 Measures of quality L/ℓ and $|B/L|$ of Tschebychev's straight-line approximations as functions of $\varrho = r/\ell$

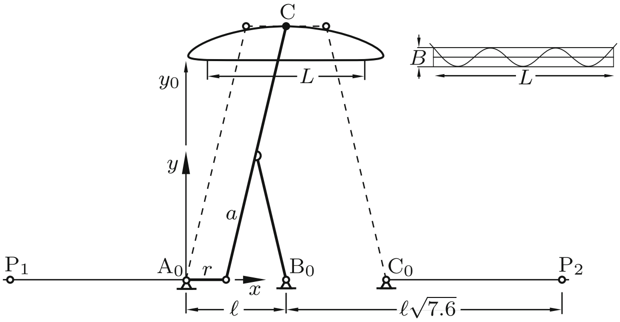

Fig. 17.38 Tschebyschev's straight-line approximation. Solid lines: Crank-rocker with $r = .4\ell$, $a = 1.3\ell$. Approximation of the line $y_0 \approx 2,19\ell$. Measures of quality $L/\ell \approx 1.44$, $|B/L| \approx .00020$. In dashed lines the cognate four-bar generating the same coupler curve. For P_1 and P_2 see the text following (17.100)

17.13 Peaucellier Inversor

Until after Tschebychev's work on straight-line approximations it was taken for granted that no plane mechanism consisting of rigid links with rotary joints could possibly generate an exact straight line. It caused, therefore, quite a sensation when in 1864 Peaucellier [33] invented a simple mechanism achieving just this[13]. The mechanism which became known as Peaucellier inversor is shown in Fig. 17.39 . It has two fixed points 0 and A a distance a apart. A crank of length ϱ connects A to the point called P . This point P is connected to 0 via two rods of equal length b and four rods of equal length $c < b$. The trajectory of P is the circle k with the equation

$$(x - a)^2 + y^2 = \varrho^2 \ . \tag{17.177}$$

[13] The history of this invention see in Sylvester [38], v.3

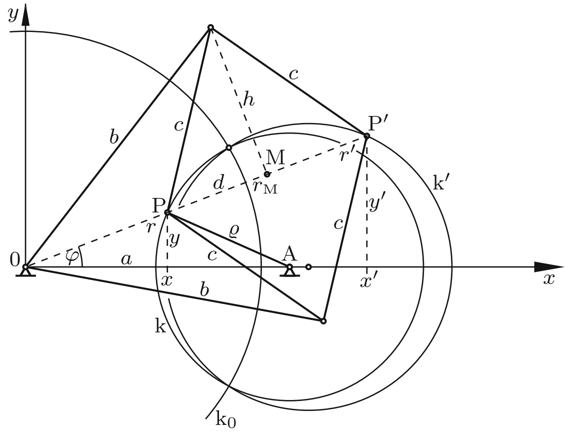

Fig. 17.39 Peaucellier inversor. Coordinates r, φ, x, y, r', x', y'. Circles k, k_0, k'

In what follows, the trajectory of P' is investigated. First, relationships between the polar coordinates of P and P' are established. Both points have equal polar coordinates φ, but different polar coordinates r and r'. The relationship between r and r' is established as follows. In terms of r_{M} (polar coordinate of M) and of auxiliary lengths d and h the polar coordinates are $r = r_{\mathrm{M}} - d$ and $r' = r_{\mathrm{M}} + d$. Hence $rr' = r_{\mathrm{M}}^2 - d^2$. Also $r_{\mathrm{M}}^2 = b^2 - h^2$ and $d^2 = c^2 - h^2$. Therefore, finally,

$$rr' = R^2 \qquad (R^2 = b^2 - c^2 = \text{ const } > 0)\ . \tag{17.178}$$

The transformation of P into P' or vice versa according to this equation is called *inversion in the circle*

$$x^2 + y^2 = R^2\ . \tag{17.179}$$

The circle itself is called inversion circle k_0. Every point of k_0 is transformed into itself. The trajectory of P' is the inverse of the circle k in k_0. Its equation is obtained as follows. Let (x, y) and (x', y') be the cartesian coordinates of P and P', respectively. The two sets of coordinates are related by the equations

$$x = x'\,\frac{r}{r'} = x'\,\frac{R^2}{r'^2} = \frac{x'R^2}{x'^2 + y'^2}\ , \qquad y = \frac{y'R^2}{x'^2 + y'^2}\ . \tag{17.180}$$

Substitution of these expressions into (17.177) results in the desired equation of the trajectory of P':

$$\left(x' - a\,\frac{R^2}{a^2 - \varrho^2}\right)^2 + y'^2 = \left(\varrho\,\frac{R^2}{a^2 - \varrho^2}\right)^2\ . \tag{17.181}$$

This is another circle centered on the x-axis. It is called the inverted circle k'. Depending on R, a and ϱ the circles k and k_0 may or may not intersect in real points. If they intersect, k' intersects the circle k_0 in the same points because every point of k_0 is transformed into itself. In Fig. 17.39 the circles intersect in two points. Let ξ be the x-coordinate of these points. Equations (17.177) and (17.179) yield

$$\xi = \frac{R^2 + a^2 - \varrho^2}{2a} \,. \tag{17.182}$$

The circle k' intersects the x-axis at the points

$$x_1 = \frac{R^2}{a + \varrho} \,, \qquad x_2 = \frac{R^2}{a - \varrho} \,. \tag{17.183}$$

In the limit $\varrho \to a$ the circle k' degenerates. Its radius, its center point coordinate as well as the point x_2 of intersection with the x-axis tend toward infinity. In contrast, the other point of intersection tends toward the finite point $x_1 = R^2/(2a)$. The point ξ tends toward the same point. Thus, the circle k' degenerates to the straight line $x = R^2/(2a)$ and to a point at infinity. In Fig. 17.40 the limiting case $\varrho = a$ is shown. Point P is moving on the circle k passing through 0, while P' is moving along the straight line $x = R^2/(2a)$. In the example shown the circles k and k_0 do not intersect. If they intersect, also the trajectory of P' passes through the points of intersection. If ϱ and a are different, but almost identical, k' is a circle of very large radius which intersects the x-axis at a point very close to $x_1 = R^2/(2a)$. In engineering such circular trajectories are as interesting as straight-line trajectories. Peaucellier's discovery inspired Hart [20], Sylvester [38] and Kempe [23] to invent other mechanisms with rotary joints which generate straight lines (see also Schoenflies/Grübler [35], Dijksman [9], Pavlin/Wohlhart [32], Demaine/O'Rourke [7]).

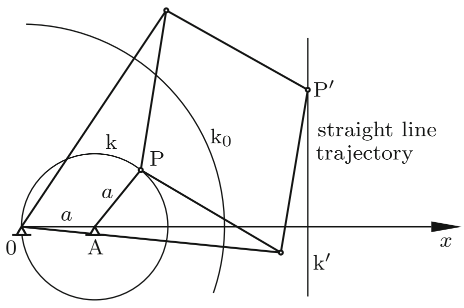

Fig. 17.40 Straight-line trajectory of P' in the special case $\varrho = a$

17.14 Four-Bars Producing Prescribed Positions of the Coupler Plane. Burmester Theory

The purpose of many linkages is to carry a planar object, i.e., a plane Σ, through an ordered set of prescribed positions $1, \ldots, n$ relative to a reference plane Σ_0. If the number n is sufficiently small, this task can be achieved by making Σ the coupler plane and Σ_0 the frame of a four-bar (as will be seen the condition is $n \leq 5$). The moving four-bar carries the plane Σ through a continuum of positions, to which the prescribed positions belong if the free design parameters are chosen properly. The complete solution to this problem which is due to Burmester [5] is the subject of this chapter. Extensive use is made of Sect. 14.5 in which fundamental concepts of Burmester were introduced. See the definitions of homologous points of points of Σ, of pole triangle, pole quadrilateral and pole curve. Burmester's basic idea is the following. The two Σ-fixed endpoints of the coupler move on circles about frame-fixed endpoints of two cranks (or rockers). Hence the problem can be stated as follows. Determine all n-tuples of homologous points $\mathrm{Q}_1, \ldots, \mathrm{Q}_n$ which are located on a circle and for each such n-tuple the center Q_0 of the circle. The line segments $\overline{\mathrm{Q}_0\mathrm{Q}_i}$ $(i = 1, \ldots, n)$ defined by each such n-tuple represent the positions of a suitable crank in the positions $\Sigma_1, \ldots, \Sigma_n$ of the coupler plane Σ. Two arbitrarily chosen n-tuples of this kind define two suitable cranks and, thus, a four-bar. Whether a four-bar thus determined produces the prescribed positions in the prescribed order remains to be seen. The problem of order is the subject of Sect. 17.14.4.

In what follows, n homologous points on a circle are called circle points, and the center of the circle is called center point. The slider-crank mechanism in Fig. 17.29a is a degenerate four-bar in that one center point Q_0 is at infinity. The circle is a straight line. The elliptic trammel in Fig. 15.4 has two sliders. In the inverted slider-crank mechanism in Fig. 17.29b and in the inverted elliptic trammel the sliders are pivoted at center points Q_0 fixed in Σ_0. The associated circle points $\mathrm{Q}_1, \ldots, \mathrm{Q}_n$ are at infinity. In the mechanism shown in Fig.15.9 one slider is pivoted in the frame Σ_0 and the other in the coupler Σ. This mechanism equals its inverse.

17.14.1 Three Prescribed Positions

Three prescribed positions can be generated by four-bars of all types including the previously listed degenerate forms. Three prescribed positions determine a pole triangle $(\mathrm{P}_{12}, \mathrm{P}_{23}, \mathrm{P}_{31})$. Since three points are always located on a circle, one out of three circle points Q_1, Q_2, Q_3 can be chosen arbitrarily. The other two circle points are then found as is shown in Fig. 14.11 by reflections in the sides of the pole triangle. The center point Q_0 is the center of the circumcircle of the triangle (Q_1,Q_2,Q_3).

Instead of a single circle point the center point Q_0 can be chosen arbitrarily. The associated circle points Q_1, Q_2, Q_3 are determined either geometrically by the pole triangle (Fig. 14.13) or analytically from (14.50). Following Fig. 14.13 special cases (a) and (b) were explained when a pole is chosen either as center point or as circle point.

Figure 14.14 explains how to determine solutions with a center point Q_0 at infinity and with circle points Q_1, Q_2, Q_3 along a straight line. The straight line is passing through the orthocenter S of the pole triangle. If the line is prescribed, the circle points are determined, and if a single circle point is prescribed, the line and the other two circle points are determined.

Figure 14.15 explains how to determine solutions with circle points lying at infinity. As center point Q_0 an arbitrary point on the circumcircle of the pole triangle can be chosen. The chosen point determines the directions $\overline{Q_0Q_i}$ $(i = 1,2,3)$ in the three positions. They are the normals to the lines $\overline{Q_0S^i}$. Instead of Q_0 the direction towards a single infinitely distant circle point, say Q_3, can be chosen. It determines the line $\overline{Q_0S^3}$ and, consequently, Q_0 and the other two directions.

17.14.2 Four Prescribed Positions. Center Point Curve. Circle Point Curves

Four prescribed positions of the coupler plane determine six poles, four pole triangles, three pole quadrilaterals and the associated pole curve p (see Figs. 14.18 and 14.22). The pole curve is the geometric locus of all points from which opposite sides of a pole quadrilateral are seen under angles which are either identical or which add up to π. The present problem is to determine all four-tuples of homologous points Q_1, Q_2, Q_3, Q_4 which are located on a circle and for each circle the center point Q_0. Following Burmester the geometric locus of all center points thus defined is called *center point curve*. Proposition: The center point curve is the pole curve. Proof: Figure 17.41 shows four homologous points Q_1, Q_2, Q_3, Q_4 on a circle with center Q_0. Homologous means that the poles of the pole quadrilateral $(P_{12},P_{23},P_{34},P_{41})$ are located somewhere on the dashed bisectors of the angles of rotation $\varphi_{ij} = \sphericalangle(Q_iP_{ij}Q_j)$ $(i,j = 1,2,3,4$ different). From Q_0 the opposite sides $\overline{P_{12}P_{23}}$ and $\overline{P_{34}P_{41}}$ are seen under the angles $\frac{1}{2}(\beta_{12}+\beta_{23})$ and $\frac{1}{2}(\beta_{34}+\beta_{41})$, respectively. Since $\beta_{12}+\beta_{23}+\beta_{34}+\beta_{41} = 2\pi$, these angles add up to π. If a pole, say P_{41}, is located on the other side of Q_0, the two opposite sides of the pole quadrilateral are seen under identical angles. End of proof.

Thus, both cranks of any four-bar capable of leading the coupler plane through four prescribed positions must be centered on the pole curve. The

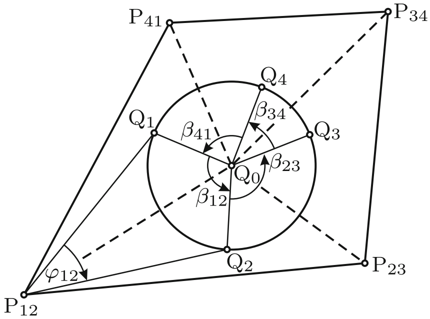

Fig. 17.41 Pole quadrilateral with four circle points and center point Q_0

problem of determining circle points associated with a chosen center point or of determining the center point associated with a chosen circle point is reduced to the previously solved problem with three prescribed positions since a solution satisfying four prescribed positions $1, 2, 3, 4$ satisfies any three positions, for example, positions $1, 2, 3$ and positions $1, 2, 4$. Hence circle points associated with a chosen center point Q_0 are determined either geometrically from pole triangles (Fig. 14.13) or analytically from Eqs.(14.50) which are now valid for the larger set of indices $i, j = 1, 2, 3, 4$ $(i \neq j)$.

Special case: As center point Q_0 a pole is chosen, for example, $Q_0 = P_{12}$. From the text following Fig. 14.13 (special case (a)) it is known that in the pole triangle associated with positions $1, 2, 3$ Q_3 is an undetermined point on the line $\overline{P_{23}P_{31}}$. For the same reason, Q_3 is an undetermined point on the line $\overline{P_{34}P_{41}}$ in the pole triangle associated with positions $1, 3, 4$. Hence Q_3 is the point of intersection of these two lines.

There is only a single solution with a center point Q_0 at infinity and with circle points Q_1, Q_2, Q_3, Q_4 along a straight line. The center point Q_0 is the infinitely distant point on the asymptote of the pole curve. The straight line is orthogonal to the asymptote. Since it is passing through the orthocenters, of all four pole triangles (see Fig. 14.14) collinearity of these orthocenters is proved.

Likewise, there is only a single solution with circle points Q_1, Q_2, Q_3, Q_4 at infinity. From Fig.14.15 it is known that the center point Q_0 is located on the circumcircles of all four pole triangles. These circles have a single point of intersection U (Fig. 14.22). As in the case of three positions, the directions $\overline{Q_0Q_i}$ $(i = 1, 2, 3, 4)$ toward the infinitely distant circle points are determined from pole triangles (Fig. 14.15). A center point Q_0 on p close to U is associated with a very long crank with very distant circle points.

Circle point curves: The geometric locus of the circle point Q_i is called *circle point curve* k_i $(i = 1, 2, 3, 4)$. If a single circle point curve, say k_1, is known, the other three curves are obtained by rotating k_1 about poles. From Fig. 14.13 and Eq.(14.50) it is known that Q_1 and Q_0 switch roles if the angles φ_{12} and φ_{13} are replaced by $-\varphi_{12}$ and $-\varphi_{13}$, respectively. This means that the pole P_{23} is replaced by its reflection P^1_{23} in the side $\overline{P_{12}P_{31}}$ of the pole triangle (see Fig. 14.12). With other indices the same is true for the other two pole triangles (P_{12},P_{24},P_{41}) and (P_{13},P_{34},P_{41}) associated with Q_1. In these triangles P_{24} and P_{34} are replaced by the reflected poles P^1_{24} and P^1_{34}, respectively. Hence the conclusion: The circle point curve k_1 is the center point curve (pole curve) associated with the six poles P_{12}, P_{13}, P_{14}, P^1_{23}, P^1_{24}, P^1_{34}. The curve passes through these six poles. It does not pass through the poles P_{23}, P_{24}, P_{34}. With indices properly changed the same is true for the circle point curves k_2, k_3 and k_4.

17.14.3 Five Prescribed Positions

Center points Q_0 are located on the center point curve associated with the four positions 1 , 2 , 3 , 4 as well as on the center point curve associated with the four positions 1 , 2 , 3 , 5. Two third-order curves have nine (real or imaginary) points of intersection. Since the curves are circular, there exist two imaginary points of intersection at infinity. This leaves seven points of intersection. Each of the two curves passes through the poles P_{12}, P_{23} und P_{31}. That these points cannot be center points Q_0 is proved by taking P_{12} as example. According to statements made earlier positions 1 , 2 , 3 , 4 require Q_3 to be the point of intersection of the lines $\overline{P_{23}P}_{31}$ and $\overline{P_{34}P}_{41}$. For the same reason, positions 1 , 2 , 3 , 5 require Q_3 to be the point of intersection of the lines $\overline{P_{23}P}_{31}$ and $\overline{P_{35}P}_{51}$. This is impossible. End of proof.

Hence either zero or two or four real points of intersection are candidates as center point Q_0, namely, those real points which are different from P_{12}, P_{23} and P_{31}. These points are called *Burmester points*. For methods of construction of these points see Müller [29]. No four-bar producing five prescribed positions exists if the number of Burmester points is zero. A single four-bar exists if the number is two and six if the number is four. This completes the solution of Burmester's problem in the case of five prescribed positions. More than five positions cannot, in general, be prescribed.

17.14.4 Crank-Rockers Producing Four Prescribed Positions in Prescribed Order

A Burmester solution for four prescribed positions is inadmissible if the four-bar produces the prescribed positions either in a wrong order or in two different configurations of the four-bar. The problem of identifying admissible solutions was first investigated by Filemon [12, 13] and since then by many researchers. A list of 170 references is given in Balli/Chand [3]. In what follows, Filemon's method of identifying all admissible crank-rockers is described.

A crank-rocker is producing four prescribed positions in the prescribed order 1 , 2 , 3 , 4 if the circle points on the crank circle are arranged in the order Q_1 , Q_2 , Q_3 , Q_4 either clockwise or counterclockwise. For this to be the case, the three triangles of circle points (Q_1,Q_2,Q_3), (Q_2,Q_3,Q_4) and (Q_3,Q_4,Q_1) must have one and the same sense. For the definition of sense of a triangle see Fig. 14.16 and the accompanying text. The sense is determined by the location of the center point Q_0 relative to the three lines of the corresponding pole triangle. Four pole triangles have altogether twelve lines dividing the infinite plane into domains. From Fig. 14.22 the following properties of the center point curve are known. The curve is intersected by lines at the six poles P_{ij} , at the six points Π_{ij} $(i, j = 1, 2, 3, 4$ different) and at no other point. From this and from Fig. 14.16 the following conclusions are drawn. When Q_0 travels on p through a pole P_{ij} $(i, j = 1, 2, 3, 4$ different), two lines belonging to one and the same pole triangle are crossed. This crossing has no effect on the sense of any triangle of circle points. In contrast, when Q_0 travels through a point Π_{ij} $(i, j = 1, 2, 3, 4$ different), two lines belonging to different pole triangles are crossed. This has the consequence that two triangles of circle points change sense. The six points Π_{ij} $(i, j = 1, 2, 3, 4$ different) divide the curve into seven sections (no matter whether the curve is unicursal or bicursal). The senses of circle point triangles do not change as long as Q_0 stays in one and the same section of the curve. Identical senses of all three circle point triangles are achieved with a set of points Q_0 which is either a single section or the union of several nonneighboring sections. In what follows, the set is denoted σ_c.

Example: In Fig. 14.22 the sense of the three circle point triangles is clockwise for points Q_0 in the unbounded section to the right of Π_{12} and in the section Π_{14}-Φ-Π_{34} . It is counterclockwise in the unbounded section to the left of Π_{23} . Thus, the set σ_c of admissible crank centers is the union of these three sections.

From Fig. 17.4b the following properties of crank-rockers are known. A four-bar is a crank-rocker if

(a) Grashof's inequality condition $\ell_{min} + \ell_{max} \le \ell' + \ell''$ is satisfied and if, in addition,

(b) the crank has the minimal length ℓ_{min} .

The angular range of a rocker consists of two disconnected sectors $< 180°$ which are arranged symmetrically with respect to the base line. For being an admissible crank-rocker a Burmester solution must satisfy condition

(c) all four circle points of the rocker must be on one and the same side of the base line, for otherwise the four prescribed positions could not be produced without disconnecting and reassembling the crank-rocker.

An algorithm determining, for a given center point curve p , all admissible crank-rockers can now be formulated as follows.

Choose an arbitrary point Q_{0r} of p and an arbitrary point Q_{0c} of the set σ_c (the indices r and c stand for rocker and crank, respectively). Determine the circle point Q_{1r} associated with Q_{0r} and the circle point Q_{1c} associated with Q_{0c}. These four points determine a four-bar in the prescribed position 1. If this four-bar does not satisfy conditions (a) and (b), choose another point Q_{0c} of the set σ_c and repeat. Otherwise, determine also the circle points Q_{2r}, Q_{3r}, Q_{4r} associated with Q_{0r} and check whether condition (c) is satisfied. If not, choose another point Q_{0c} of the set σ_c and repeat. Otherwise, Q_{0r} and Q_{0c} are centers of the rocker and of the crank of an admissible crank-rocker. The sequence of decisions thus described has to be made for every point Q_{0r} of p in combination with every point Q_{0c} of the set σ_c.

17.15 Trajectory of the Center of Mass of a Four-Bar

In Fig. 17.42a r_0, r_1, r_2, r_3 represent differences of complex numbers in the complex plane. All of them have constant absolute values. They form a quadrilateral. The relation between the four is

$$r_2 = r_1 + r_3 - r_0 \ . \tag{17.184}$$

Let it be assumed that r_0 has constant direction. Then the differences of complex numbers form a mobile four-bar with base r_0. For any coupler-fixed point C a complex constant z exists such that

$$\overline{\mathrm{A_1C}} = z r_3 \ . \tag{17.185}$$

When the four-bar is moving, the tip of the complex number

$$r_{\mathrm{C}} = r_1 + z r_3 \tag{17.186}$$

traces the coupler curve generated by C.

The moving links $i = 1, 2, 3$ have masses m_i and centers of mass S_i (Fig. 17.42b). The positions of the centers of mass on the bodies are expressed in the form

$$\varrho_i = z_i r_i \qquad (i = 1, 2, 3) \tag{17.187}$$

with complex constants z_i. Let r_{S} be the complex number representing the composite system center of mass S of the four-bar (the moving parts only). It is determined by the formula

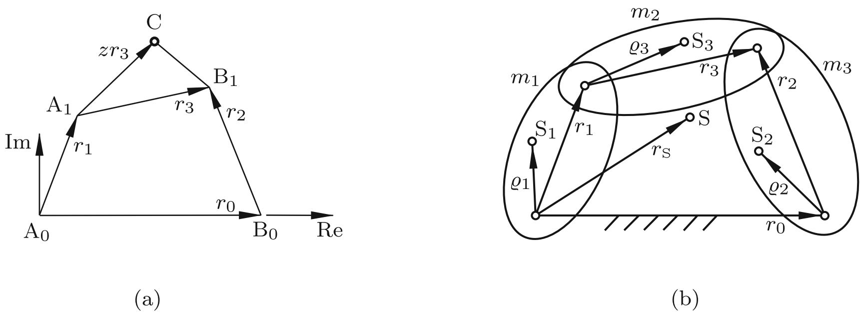

(a) (b)

Fig. 17.42 Four-bar with coupler point C **(a)** and with centers of mass **(b)**

$$\begin{aligned} r_S &= \frac{m_1\varrho_1 + m_3(r_1+\varrho_3) + m_2(r_0+\varrho_2)}{m_1+m_2+m_3} \\ &= \frac{m_1 z_1 r_1 + m_3(r_1+z_3 r_3) + m_2[r_0 + z_2(r_1+r_3-r_0)]}{m_1+m_2+m_3} \\ &= \frac{(m_1z_1+m_2z_2+m_3)r_1 + (m_2z_2+m_3z_3)r_3 + m_2(1-z_2)r_0}{m_1+m_2+m_3} \; . \end{aligned} \tag{17.188}$$

In the general case $m_1z_1+m_2z_2+m_3 \neq 0$,

$$r_S = \frac{m_1z_1+m_2z_2+m_3}{m_1+m_2+m_3}\left(r_1 + \frac{m_2z_2+m_3z_3}{m_1z_1+m_2z_2+m_3}\,r_3\right) + \frac{m_2(1-z_2)r_0}{m_1+m_2+m_3} \; . \tag{17.189}$$

The term in parentheses has the form (17.186) with

$$z = \frac{m_2z_2+m_3z_3}{m_1z_1+m_2z_2+m_3} \; . \tag{17.190}$$

The complex number r_C moves along the coupler curve of the coupler-fixed point C specified by this constant z. The constant complex factor in front has the effect of a stretch-rotation of this coupler curve and the constant behind has the effect of a translatory displacement. Hence the trajectory of the composite center of mass of a moving four-bar is similar to a uniquely determined coupler curve of the four-bar.

The acceleration of the composite center of mass determines the resultant inertia force acting on the base of the four-bar. The resultant force is zero throughout the motion if (17.188) yields $r_S =$ const. This is the case under the weak conditions

$$m_1z_1+m_2z_2+m_3 = 0 \; , \qquad m_2z_2+m_3z_3 = 0 \; . \tag{17.191}$$

In these conditions the link lengths do not appear. The four link lengths, the three masses and, in addition, the position of the center of mass on a single link, for example, the number z_3, can be chosen arbitrarily. Both conditions are satisfied if the centers of mass on the other two bodies satisfy the conditions

$$z_1 = \frac{m_3}{m_1}(z_3 - 1) , \qquad z_2 = -\frac{m_3}{m_2} z_3 . \tag{17.192}$$

Note that for producing the time-varying angular acceleration of the coupler a torque is required. Even if the conditions (17.191) are satisfied this torque causes time-varying forces of equal magnitude and opposite directions acting on the base in the crank bearings.

References

1. Artobolevski I I (1964) Mechanisms for the generation of plane curves. Pergamon Press, Oxford
2. Artobolevski I I, Levitski N I, Cherkudinov S A (1959) Synthesis of plane mechanisms (Russ.). Isdat.Phys.-Mat. Lit., Moscow
3. Balli S S, Chand S (2002) Defects in link mechanisms and solution rectification. Mechanism Machine Theory 37:851–876
4. Brossard J P (2006) Dynamique du véhicule - Modélisation des systèmes complexes, Presses Polytechniques et universitaires Romandes
5. Burmester L (1888) Lehrbuch der Kinematik. Felix,Leipzig
6. Cayley A (1889) The collected mathematical papers of Arthur Cayley, v.1–13. Cambridge: The Univ. Press; (1963) Johnson Reprint Co., New York
7. Demaine E D , O'Rourke J (2007) Geometric folding algorithms. Linkages, origami, polyhedra. Cambridge Univ. Press
8. Dijksman E A (1969) Coordination of coupler-point positions and crank rotations in connection with Roberts' configuration. Trans ASME 91B:55–65
9. Dijksman E A (1975) Kempe's linkages and their derivations. J. Eng. Ind. 97B:801–808
10. Dijksman E A (1976) Motion geometry of mechanisms. Cambridge Univ. Press,
11. Erdman A G (ed.) (1993) Modern kinematics. Developments in the last forty years. Wiley, New York (appr. 2250 literature references)
12. Filemon E: Marking points for crank-rocker linkage on the centerpoint curve. Periodika Polytechnica XV:287–291
13. Filemon E (1972) Useful ranges of centerpoint curves for design of crank-and-rocker linkages. Mechanism Machine Theory 7:47–53
14. Freudenstein F (1956) On the maximum and minimum velocities and the accelerations in four-link mechanisms. Trans. ASME 78:779–787
15. Freudenstein F (1959) Structural error analysis in plane kinematics synthesis. Trans ASME 81B:15–22
16. Geronimus Ya. L. (1962) Geometric apparatus of the theory of synthesis of planar mechanisms (russ.). Gos. Isd. Physico-Math. Lit. Moscow
17. Grashof F (1883) Theoretische Maschinenlehre v.2. (1875 v.1, 1890 v.3). Voss, Leipzig
18. Hain K (1967) Atlas für Getriebe-Konstruktionen Bd.1,2. Vieweg, Braunschweig
19. Hain K (1961) Angewandte Getriebelehre. VDI-Verl., Düsseldorf. Engl. trans. (1968) Applied kinematics. 2nd ed. McGraw Hill, New York
20. Hart H (1875) A parallel motion. Proc.London Math.Soc.6:137–139
21. Hayes M J O, Husty M L (2003) On the kinematic constraint surfaces of general three-legged planar robot platforms. Mechanism Machine Theory 38:379–394
22. Hrones J A, Nelson G L (1951) Analysis of the four-bar linkage. Wiley, New York
23. Kempe A B (1875) On a general method of producing exact rectilinear motion by linkworks. Proc.Roy.Soc.London 23:565–577

24. Klein F, Müller C (eds.) (1901-1908) Enzyklopädie der Math. Wissenschaften. v.IV: Mechanik. Teubner, Leipzig
25. Kraus R (1956) Geradführungen durch das Gelenkviereck. VDI-Verl., Düsseldorf
26. Lichtenheldt W, Luck K (1979) Konstruktionslehre der Getriebe. Akademie-Verl., Berlin
27. Mayer A E (1938) Koppelkurven mit drei Spitzen und spezielle Koppelkurvenbüschel. Mathematische Zeitschrift 43:389–445
28. Müller R (1891) Über die Doppelpunkte der Koppelkurve. Z. Mathematik Physik 36:65–70. Engl.Transl. (1962) On the double points of coupler curves. Kansas State Univ. Bull. 46, Special Report 21:14–22
29. Müller R (1892) Konstruktion der Burmesterschen Punkte für ein ebenes Gelenkviereck. Z. Mathematik Physik 37:213–217 and (1893) 38:129–147
30. Müller R (1897) Beiträge zur Theorie des ebenen Gelenkvierecks. Z. Mathematik Physik 42:247–271. Engl.Transl. (1962) Contributions to the theory of the planar four-bar. Kansas State Univ. Bull. 46, Special Report 21:135–168
31. Müller R (1901) Die Koppelkurve mit sechspunktig berührender Tangente. Z. Mathematik Physik 46:330–342. Engl.Transl. (1962) The coupler curve with six-point osculating tangent. Kansas State Univ. Bull. 46, Special Report 21:178–194
32. Pavlin G, Wohlhart K (1992) On straigh-line space mechanisms. Proc. 6th Int. IFToMM Conf.:241–246
33. Peaucellier N (1874) Transformation du mouvement circulaire en mouvement rectiligne. Revue Scientif.4:499
34. Powell M J D (1981) Approximation theory and methods. Cambridge Univ.Press
35. Schoenflies A, Grübler M (1908) Kinematik. In: [24]:190–278
36. Soni A H (1974) Mechanism synthesis and analysis. Mac-Graw Hill, New York
37. Suh C H (1967) Design of space mechanisms for function generation. J. Eng.f.Ind. 89B:507–512
38. Sylvester J J (1904/08/09/12) The collected mathematical papers of James Joseph Sylvester, v.1–4. Chelsea, New York
39. Tschebychev P L (1961) Oeuvres de P.L. Tchebychef, v.I. Dover, New York. Théorie des mécanismes connus sous le nom de parallélogrammes. pp.111–143. Sur les questions de minima qui se rattachent à la représentation approximative des fonctions. pp.273–378.
40. Tschebychev P L (1962) Oeuvres de P.L. Tchebychef, v.II. Chelsea, New York. Sur un mécanisme. pp.51-57. Les plus simples systèmes de tiges articulées. pp.273–281. Sur les parallélogrammes composés de trois éléments et symétriques par rapport à un axe. pp.285–297. Sur les parallèlogrammes composés de trois éléments quelconques. pp.301–331. Sur le système articulé le plus simple donnant des mouvements symétriques par rapport à un axe. pp.495–540
41. Volmer J (1956/57) Ein Beitrag zur Erzeugung von Koppelkurven. Wiss.Z.Dresden 6:491–510
42. Volmer J (ed.) (1976) Autorenkollektiv: Getriebetechnik – Lehrbuch VEB, Berlin
43. Volmer J (ed.) (1979) Getriebetechnik-Koppelgetriebe. VEB, Berlin
44. Volmer J (ed.) (1992) Getriebetechnik-Grundlagen. Verl. Technik, Berlin
45. Watson G A (1980) Approximation theory and numerical methods. Wiley, New York
46. Wunderlich W (1970) Ebene Kinematik. BI-Verl. Mannheim